Trailer control through vehicle yaw moment control: theoretical analysis and experimental assessment

ZANCHETTA, Mattia, TAVERNINI, Davide, SORNIOTTI, Aldo, GRUBER, Patrick, LENZO, Basilio <http://orcid.org/0000-0002-8520-7953>, FERRARA, Antonella, SANNEN, Koen, DE SMET, Jasper and DE NIJS, Wouter

Published version

ZANCHETTA, Mattia, TAVERNINI, Davide, SORNIOTTI, Aldo, GRUBER, Patrick, LENZO, Basilio, FERRARA, Antonella, SANNEN, Koen, DE SMET, Jasper and DE NIJS, Wouter (2019). Trailer control through vehicle yaw moment control: theoretical analysis and experimental assessment. Mechatronics, 64 (102282).

Mechatronics 64 (2019) 102282

Contents lists available at ScienceDirect

Mechatronics

journal homepage: www.elsevier.com/locate/mechatronics

Trailer control through vehicle yaw moment control: Theoretical analysis and experimental assessment ☆

Mattia Zanchetta [a], Davide Tavernini [a], Aldo Sorniotti [a,*], Patrick Gruber [a], Basilio Lenzo [b], Antonella Ferrara [c], Koen Sannen [d], Jasper De Smet [d], Wouter De Nijs [d]

[a] University of Surrey, Guildford, UK
[b] Sheffield Hallam University, Sheffield, UK
[c] Universita' di Pavia, Pavia, Italy
[d] Flanders MAKE, Lommel, Belgium

ARTICLE INFO

Keywords:
Torque-vectoring
Articulated vehicle
Hitch angle control
Yaw moment
Experimental tests
Performance comparison

ABSTRACT

This paper investigates a torque-vectoring formulation for the combined control of the yaw rate and hitch angle of an articulated vehicle through a direct yaw moment generated on the towing car. The formulation is based on a single-input single-output feedback control structure, in which the reference yaw rate for the car is modified when the incipient instability of the trailer is detected with a hitch angle sensor. The design of the hitch angle controller is described, including the gain scheduling as a function of vehicle speed. The controller performance is assessed by means of frequency domain and phase plane analyses, and compared with that of an industrial trailer sway mitigation algorithm. In addition, the novel control strategy is implemented in a high-fidelity articulated vehicle model for robustness assessment, and experimentally tested on an electric vehicle demonstrator with four on-board drivetrains, towing two different conventional single-axle trailers. The results show that: (i) the torque-vectoring controller based only on the yaw rate of the car is not sufficient to mitigate trailer instability in extreme conditions; and (ii) the proposed controller provides safe trailer behaviour during the comprehensive set of manoeuvres, thus justifying the additional hardware complexity associated with the hitch angle measurement.

1. Introduction

Articulated vehicle dynamics are more complex than those of rigid vehicles, and involve several safety-critical situations. For instance, trailer snaking and jackknifing are conditions that untrained drivers are not able to control [1] and may lead to severe accidents. As a result, many studies discuss the dynamic behaviour of articulated vehicles and propose ways to mitigate their potentially unstable response.

For example, [2–5] investigate the stability properties of different tractor-trailer combinations through simulations. The common conclusion is that the stability of the overall vehicle depends on the trailer parameters (e.g., mass, yaw mass moment inertia and dimensions) and how the trailer is connected to the tractor. Nowadays the towing vehicle itself is not normally a source of instability, because it is controlled by the vehicle stability controller based on the actuation of the friction brakes. On the other hand, in general the trailer is not directly controlled. The importance of the trailer connection is discussed by Sharp and Fernández [6], who analyse the influence of the position and friction level of the hitch joint.

In the literature the position of the centre of gravity (COG) of the trailer and the location of the trailer axle with respect to the hitch joint are mentioned as the key parameters for articulated vehicle stability, i.e., they determine whether the vehicle is subject to common instability modes, such as snaking and jackknifing. In particular, jackknifing instability is described by Bouteldja and Cerezo in [7] as "a loss of stability in the yaw motion of the articulated system […]. The driving wheels of the tractor lose their skid resistance and are involved towards the right-hand side or the left because of the force exerted by the trailer." The work of the same author in [8] describes a jackknifing detection system for heavy-duty vehicles. Snaking occurs when the system is subject to an oscillatory behaviour, and can be predicted from the real part of the system eigenvalues. This is the focus of the study by Azad et al. [9], which also considers the effect of the damping coefficient of the hitch joint. Darling et al. and Šušteršič et al. [10–11] experimentally assess the main trailer parameters provoking instability at high speed, such as the position of the centre of gravity of the trailer.

Several methods are proposed to improve articulated vehicle stability by controlling the towing vehicle. For example, car manufacturers

☆ This paper was recommended for publication by Associate Editor Dr. Amir Khajepour.

* Corresponding author.
E-mail address: a.sorniotti@surrey.ac.uk (A. Sorniotti).

https://doi.org/10.1016/j.mechatronics.2019.102282
Received 4 February 2019; Received in revised form 17 September 2019; Accepted 27 September 2019

List of symbols

$a_{B,\,i}$, $b_{B,\,i}$	Butterworth filter coefficients for the industrial controller, $i = 0, 1, 2$
a_C	front semi-wheelbase of the car
$a_{x,\,C}$	longitudinal acceleration of the car
$a_{y,\,C}$	lateral acceleration of the car
$a_{y,\,T}$	lateral acceleration of the trailer
a_T	longitudinal distance between the trailer centre of gravity and the hitch joint
B	Butterworth filter transfer function
b_C	rear semi-wheelbase of the car
b_T	longitudinal distance between the trailer axle and the trailer centre of gravity
C_{Drag}	aerodynamic drag coefficient
C_{PI}	proportional integral controller transfer function
C_i	i axle cornering stiffness, $i = F, R, T$
D_i	coefficients in the denominator of the transfer functions, $i = 0, 1, 2, 3, 4$
e_C	longitudinal distance from the hitch joint to the rear axle of the car
f_{max}	maximum steering frequency achieved during the sweep steer test
f_n	natural frequency of the system
$F_{y,\,ij}$	lateral tyre force in the nonlinear model, $i = L, R$; $j = F, R, T$
$F_{y,\,F}$	lateral force at the front axle of the car
$F_{y,\,R}$	lateral force at the rear axle of the car
$F_{y,\,T}$	lateral axle force of the trailer
$F_{z,\,ij}$	vertical tyre force, $i = L, R$; $j = F, R, T$
$F_{z,\,i,\,static}$	static load on the i-th axle, $i = F, R, T$
$G_{i,\,j}$	transfer functions for the articulated vehicle, $i = \delta_w, M_{z,\,ref}$; $j = r_C, \beta_C, \phi$
$G_{M_{z,ref},r_C,iso}$	yaw moment to yaw rate transfer function for the isolated vehicle
h_C	longitudinal distance from the hitch joint to the centre of gravity of the car
$H_{CG,\,C}$	height of the centre of gravity of the towing car
H_{Hitch}	height of the hitch joint
$H_{RC,\,C}$	roll centre height of the car
$H_{RC,\,T}$	roll centre height of the trailer
$H_{Roll,\,C}$	vertical distance from the centre of gravity to the roll centre of the car
$H_{Roll,\,T}$	vertical distance from the centre of gravity to the roll centre of the trailer
i,j	generic index
$IACA$	integral of the absolute value of the control action
$J_{z,\,C}$	yaw mass moment of inertia of the car
$J_{z,\,T}$	yaw mass moment of inertia of the trailer
$k_{Roll,\,F}$	front axle roll stiffness of the car
$k_{Roll,\,R}$	rear axle roll stiffness of the car
K_{aw}	anti-windup gain
K_{Ir}	integral gain of the PI controller
K_{Pr}	proportional gain of the PI controller
K_β	weighting coefficient for the yaw rate reference based on the sideslip angle
K_ϕ	weighting coefficient for the yaw rate error and hitch angle error
$K_{\phi,\,min}$	minimum value of the weighting coefficient of yaw rate error and hitch angle error
k_1	coefficient for the calculation of the aerodynamic load transfer
k_2	coefficient for the calculation of the load transfer associated with the lateral acceleration
l_C	wheelbase of the towing car
l_T	distance from the trailer axle to the hitch joint
m_C	mass of the car
m_T	mass of the trailer
$M_{z,\,ref}$	reference yaw moment
$M_{z,pre-sat}$	reference yaw moment before saturation
$N_{ij,\,k}$	numerator coefficients of the transfer functions, $i = 0, 1, 2, 3$; $j = \delta_w, M_{z,\,ref}$; $k = r_C, \beta_C, \phi$
$OLTF_{art,K_\phi=0}$	open-loop transfer function of the articulated vehicle, with $K_\phi = 0$
$OLTF_{art,K_\phi=1}$	open-loop transfer function of the articulated vehicle, with $K_\phi = 1$
$OLTF_{iso}$	open-loop transfer function of the isolated vehicle
r_C	yaw rate of the towing car
r_h	handling yaw rate
r_s	stability yaw rate
r_{ref}	reference yaw rate
$RMSE_i$	root mean square error, $i = \Delta\phi, \Delta r, \Delta r_\phi$
s	Laplace operator
S_C	car frontal area
t	time
t_f	final time of the relevant part of the manoeuvre for the computation of the performance indicators
t_i	initial time of the relevant part of the manoeuvre for the computation of the performance indicators
t^-	time at the previous discretisation step
T_i	track width, $i = F, R, T$
$T_{ref,\,ij}$	reference motor torque, $i = L, R$; $j = F, R$
V	vehicle speed
V_{in}	initial vehicle speed
v_x	longitudinal velocity of the car
v_y	lateral velocity of the car
W_ϕ	hitch angle error gain
X	axis of the inertial reference system
Y	axis of the inertial reference system
z	complex number in the Z-transform process
α_i	axle slip angles, $i = F, R, T$
β_C	sideslip angle at the centre of gravity of the car
$\beta_{C,\,R}$	sideslip angle at the rear axle of the car
β_{Dat}	sideslip angle of the car measured by the Corrsys-Datron sensor at the front bumper
δ_{swa}	steering wheel angle
δ_w	steering angle of the front wheels of the car
$\Delta F_{z,\,aero}$	longitudinal load transfer due to aerodynamic forces
$\Delta F_{z,a_y,i}$	lateral load transfer on each axle caused by the lateral acceleration, $i = F, R, T$
Δr_C	car yaw rate error
$\Delta r_{C,\,filt,\,B}$	filtered yaw rate error of the car in the industrial controller
Δr_ϕ	yaw rate error with hitch angle correction
$\Delta\phi$	hitch angle error
$\Delta\phi_{lim}$	hitch angle error threshold for the full activation of the hitch angle contribution
$\Delta\phi_{sat}$	saturation value of the hitch angle error
$\Delta\phi_{th}$	lower activation threshold of the hitch angle contribution
ζ	damping ratio of the transfer function
μ	tyre-road friction coefficient
ρ	air density
ϕ	hitch angle
ϕ_{max}	maximum value of hitch angle during the test
ϕ_{ref}	reference hitch angle

(e.g., Mercedes, Honda and Skoda, see [12–14]) are offering a dedicated trailer stability function in the electronic stability program (ESP) of their production cars, which activates when a trailer is attached. In case of potentially dangerous trailer oscillations, the algorithm intervenes, e.g., by reducing the engine torque and actuating the friction brakes on the towing vehicle (either the front brakes individually or all four brakes) to slow down and stabilise the car-trailer combination. Also Gerum et al. [15] discuss the possibility of improving stability by applying braking torques at the rear wheels of the towing vehicle. The patent by Wu et al. in [16] proposes the application of symmetric and asymmetric friction braking torques based on the estimated motion of the trailer, to create a yaw moment to damp trailer sway. A typical braking algorithm for the towing vehicle to mitigate the trailer oscillations is described by Williams and Mohn [17]. The oscillations are detected from the difference between a quasi-static prediction of the yaw rate of the car and the actual yaw rate, which is band-pass filtered with appropriate corner frequencies to highlight the oscillations caused by the trailer, usually ranging between 0.5 Hz and 2 Hz. The authors conclude that the system works well but further analysis is required for the algorithm industrialisation. Hac et al. [18] study the stability of car-trailer systems through analytical modelling, simulation and road testing. In addition, the effects of applying symmetric or asymmetric braking control on the towing vehicle are analysed with simulations. An important conclusion of this study is that asymmetric braking is more effective in trailer stabilisation than symmetric braking, because of the direct yaw moment that is generated by the controller. In [19] Mokhiamar and Abe propose two sliding mode formulations for direct yaw moment control, one based on the yaw rate of the towing vehicle and the other one on its sideslip angle. In [20] Mokhiamar also introduces a feedback controller that outputs the desired yaw moment and lateral force, which are then converted into braking force and steering demands for the towing vehicle. The combined controller is less effective in low friction conditions. Feedback controllers to obtain a stabilising steering input for the rear wheels of the towing vehicle are compared by Deng and Kang in [21]. The investigated strategies are based on the yaw rate and lateral velocity of the tractor, or hitch angle and hitch rate, or their combination. The study highlights that the operating point for model linearization has little influence on the stability properties of the system, i.e., on the poles in the complex plane.

Several studies apply the control action only to the trailer. In [22] Fernández and Sharp propose an active braking system for caravans, which uses the measured hitch angle and its time derivative to obtain asymmetric braking pressure demands to damp the hitch angle oscillations. From the measurement of the trailer roll rate, which is integrated along time and filtered, the controller from Sharp and Fernández [23] computes a braking torque demand for either the right or left wheels of the trailer. The results highlight the roll motion of the articulated vehicle as a key contributor to vehicle behaviour leading to snaking instability, which justifies the possibility of designing a roll-based controller. In [24] Plöchl et al. present a sliding mode controller that computes a corrective yaw moment and individual braking torques for the trailer, based on measurements of the yaw rates of the trailer and towing vehicle. The study also shows the robustness of the developed controller and the ability to allow safe vehicle operation at higher speed values. As an alternative to brake interventions, in [25] Tabatabaei Oreh et al. discuss active steering control of the trailer wheels to track a reference hitch angle. The study focuses on the design of the reference vehicle behaviour and shows that that the proposed controller can provide superior tracking performance in comparison with other considered strategies. In [26] Lee et al. describe a controller for the braking system of the trailer, which is robust with respect to sensor noise as well as variations in longitudinal velocity and model parameters. In [27] Shamim et al. compare three linear quadratic regulators (LQRs) for car-trailer stabilisation, based on: (i) active trailer braking control; (ii) active trailer steering control; and (iii) a variable geometry approach, i.e., the lateral position of the hitch joint is actively controlled. The simulation results from a linear single-track vehicle model show that option (iii) is the least effective.

Other studies discuss control systems with concurrent actuations on tractor and trailer. For example, in [28] Oh et al. describe a stability controller for a combination vehicle. The system actuates the individual brakes of the car and trailer based on the hitch angle, yaw rate, roll angle, roll rate and lateral acceleration of the tractor. The controller also includes state estimation and is shown to improve the vehicle behaviour in several simulated manoeuvres. In [29] Tamaddoni and Taheri present an adaptive controller actuating the tractor and trailer brakes through the direct Lyapunov method, including validation with TruckSim simulations. The authors mention the possibility of integrating the system with a standard anti-lock braking system (ABS). In [30] Ei-Gindy et al. compare LQRs actuating the brakes of: (i) the towing vehicle, i.e., a truck; (ii) the dolly, i.e., the second articulated unit, connecting the truck with the trailer; and (iii) the trailer. The results highlight the benefits of the control strategies, although the authors mention robustness issues with respect to model parameter variations. LQRs for the steering actuation are simulated by Kim et al. in [31]. Steering control is implemented on the rear axle of the tractor and trailer wheels, as a function of the yaw rates and sideslip angles of the towing vehicle and trailer. The results show improvements in sharp cornering manoeuvres. The patent by Englert et al. [32] describes an active braking system based on the detection of trailer sway. Wang et al. [33] consider a single-track model of the articulated vehicle and study the effect of external yaw moments on the towing vehicle and trailer, based on a PID controller that uses the yaw rate of the passive vehicle as reference. The results show that the concurrent control of trailer and tractor can provide benefits with respect to controlling either unit alone. In [34] Chen and Shieh conduct experimental tests on a small-scale articulated vehicle purposely built to study a model reference adaptive controller preventing jackknifing. However, the small scale of the vehicle prototype, with very different tyres and suspensions from those of an actual vehicle, would require a further validation of the controller.

In the literature, the majority of the direct yaw moment controllers for articulated vehicles uses the friction brakes, which inevitably reduce vehicle speed, and thus are actuated only in emergency conditions. Torque-vectoring (TV) represents an alternative to achieve the benefits of direct yaw moment control without penalising drivability. The studies in [35–41] offer an overview on the advantages of TV on rigid vehicles with multiple electric motors, in terms of cornering performance and energy efficiency. TV enables direct yaw moment control without significant reduction of vehicle speed, which is the typical issue of the interventions of common vehicle stability controllers actuating the friction brakes. In the field of articulated vehicles, the patent from Wu [42] describes a TV strategy for the stabilisation of a car-trailer system. The controller splits the torque among the rear wheels of the towing vehicle in accordance to the trailer sway, which is detected with a band-pass filter applied to the yaw rate of the towing vehicle, similarly to the algorithms in [16] and [17]. One of the conclusions of the review from Vempaty and He [43] is that there is a lack of published experimental results of TV controllers on full-size articulated vehicles. Even more importantly, the literature misses an assessment of the benefits of directly including the hitch angle input into the trailer sway mitigation algorithm, with respect to the currently implemented industrial formulations (see [12–14,16,17,42]), based on the control of the filtered yaw rate of the towing vehicle.

This study provides further insights to address this knowledge gap. The main contributions are:

- A dedicated TV control function for trailer stability, designed for an electric car with multiple motors towing a conventional trailer. The TV controller includes: (i) the continuous feedback control of the car yaw rate; and (ii) the control of the measured hitch angle in case of significant trailer oscillations.

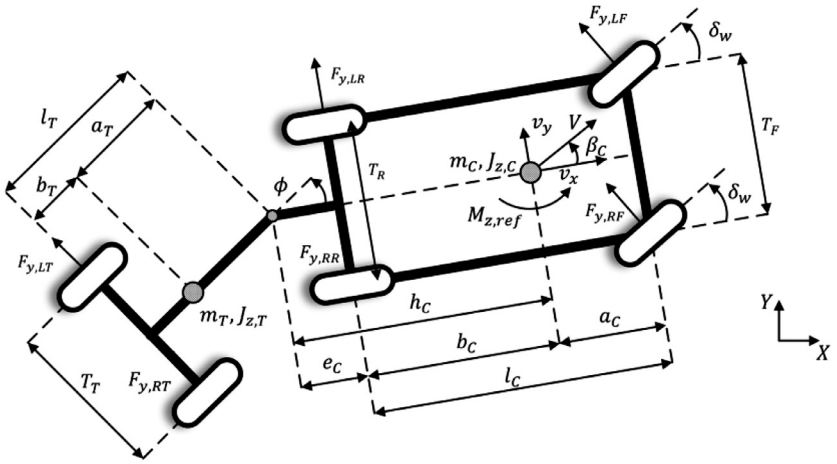

Fig. 1. Double-track model of the articulated vehicle. All variables are shown with a positive sign.

- A single input single output (SISO) formulation for the control of the two relevant variables, i.e., the yaw rate and hitch angle, with one control action, i.e., the direct yaw moment applied to the car.

The paper is structured as follows. The vehicle models for control system design and assessment are explained in Section 2. Section 3 describes the proposed hitch angle control algorithm. Sections 4–6 analyse the controller performance with simulations and experimental tests on a four-wheel-drive electric vehicle demonstrator. In Section 4, phase plane and frequency domain analyses are used to assess the benefits of the proposed controller with respect to an industrial trailer sway mitigation algorithm for stability control systems of passenger cars, based on a band-pass filter applied to the yaw rate of the towing vehicle. The simulations in Section 5 demonstrate the controller capability of mitigating jackknifing and snaking, and its robustness with respect to significant vehicle parameter variations. Section 6 presents the experimental assessment of the controller along several manoeuvres at the Lommel proving ground (Belgium). Finally, Section 7 draws the main conclusions.

2. Articulated vehicle models

2.1. Vehicle model for phase plane analysis

Fig. 1 reports the schematic of the simplified nonlinear double-track model of the articulated vehicle, adopted for the phase plane analyses. The model includes four states, namely: (i) the car sideslip angle, β_C; (ii) the car yaw rate, r_C; (iii) the hitch rate, $\dot{\phi}$; and (iv) the hitch angle, ϕ, i.e., the angle between the longitudinal axes of the car and the trailer. The two model inputs are: (i) the steering angle on the front axle of the car, δ_w, imposed by a human driver or an automated driving controller; and (ii) the direct yaw moment applied to the car, $M_{z,\,ref}$, which is computed by the TV controller, and generated by the torque difference between the electric motors on the left and right vehicle sides.

By assuming that ϕ, β_C and δ_w are small, the resulting equations of motion in matrix form are [44]:

$$\begin{bmatrix} (m_C+m_T)V & -m_T(h_C+a_T) & -m_T a_T & 0 \\ -m_T h_C V & J_{z,C}+m_T h_C(h_C+a_T) & m_T h_C a_T & 0 \\ -m_T a_T V & J_{z,T}+m_T a_T(h_C+a_T) & J_{z,T}+m_T a_T^2 & 0 \\ 0 & 0 & 0 & 1 \end{bmatrix} \begin{bmatrix} \dot{\beta}_C \\ \dot{r}_C \\ \ddot{\phi} \\ \dot{\phi} \end{bmatrix} = \begin{bmatrix} F_{y,F}+F_{y,R}+F_{y,T}-(m_C+m_T)V r_C \\ a_C F_{y,F}-b_C F_{y,R}-h_C F_{y,T}+m_T h_C V r_C+M_{z,ref} \\ -l_T F_{y,T}+m_T a_T V r_C \\ \dot{\phi} \end{bmatrix} \tag{1}$$

where:

$$F_{y,j}=F_{y,Lj}+F_{y,Rj} \quad j=F,R,T \tag{2}$$

The lateral tyre forces are computed with the Pacejka Magic Formula, without considering the interaction between longitudinal and lateral forces [45]:

$$F_{y,ij}(t)=F_y(\alpha_j, F_{z,ij}, \mu), \quad i=L,R,\ j=F,R,T \tag{3}$$

where the slip angles, in accordance to [44] and [46], are given by:

$$\alpha_F=\frac{1}{v_x}(v_y+a_C r_C)-\delta_w \cong \beta_C+\frac{a_C r_C}{V}-\delta_w \tag{4}$$

$$\alpha_R=\frac{1}{v_x}(v_y-b_C r_C) \cong \beta_C-\frac{b_C r_C}{V} \tag{5}$$

$$\alpha_T=\frac{1}{v_x}(v_y-(h_C+l_T)r_C-l_T\dot{\phi})-\phi \cong \beta_C-\frac{(h_C+l_T)r_C}{V}-\frac{l_T}{V}\dot{\phi}-\phi \tag{6}$$

In the calculation of $F_{z,\,ij}$, the nonlinear model considers the load transfers due to the aerodynamic drag and lateral acceleration a_y. The load transfer associated with the longitudinal vehicle acceleration is neglected, as the phase plane analyses are run at constant speed. In formulas:

$$F_{z,ij}=\frac{F_{z,j,\ static}}{2}+k_1\frac{\Delta F_{z,aero}}{2}+k_2\Delta F_{z,a_y,j},\ i=L,R,$$
$$j=F,R,T,\begin{cases} k_1=-1\ if\ j=F \\ k_1=1\ if\ j=R \\ k_1=0\ if\ j=T \end{cases},\ \begin{cases} k_2=-1\ if\ i=L \\ k_2=1\ if\ i=R \end{cases} \tag{7}$$

where:

$$\Delta F_{z,aero}=\frac{1}{2}\rho S_C C_{Drag} V^2 \frac{H_{CG,C}}{l_C} \tag{8}$$

$$\Delta F_{z,a_y,F}=\frac{m_C a_{y,C}}{T_F}\left(\frac{b_C H_{RC,C}}{l_C}+\frac{k_{Roll,F}H_{Roll,C}}{k_{Roll,F}+k_{Roll,R}}\right)+\frac{m_T a_{y,T} b_T}{T_F l_T}\left(\frac{b_C H_{RC,C}}{l_C}\left(1-\frac{h_C}{b_C}\right)+\frac{k_{Roll,F}(H_{Hitch}-H_{RC,C})}{k_{Roll,F}+k_{Roll,R}}\right) \tag{9}$$

$$\Delta F_{z,a_y,R}=\frac{m_C a_{y,C}}{T_R}\left(\frac{a_C H_{RC,C}}{l_C}+\frac{k_{Roll,R}H_{Roll,C}}{k_{Roll,F}+k_{Roll,R}}\right)+\frac{m_T a_{y,T} b_T}{T_R l_T}\left(\frac{a_C H_{RC,C}}{l_C}\left(1+\frac{h_C}{a_C}\right)+\frac{k_{Roll,R}(H_{Hitch}-H_{RC,C})}{k_{Roll,F}+k_{Roll,R}}\right) \tag{10}$$

$$\Delta F_{z,a_y,T}=\frac{m_T a_{y,T}}{T_T}\left(\frac{a_T H_{RC,T}}{l_T}+H_{Roll,T}-\frac{b_T}{l_T}(H_{Hitch}-H_{RC,T})\right) \tag{11}$$

Table 1
Main vehicle demonstrator parameters.

	Car	
Mass [kg]	2290	
Yaw mass moment of inertia [kgm^2]	2761	
Wheelbase [m]	2.660	
Front semi-wheelbase [m]	1.399	
Longitudinal distance from rear axle to hitch joint [m]	0.850	
Track width [m]	1.625	
Longitudinal distance from the Corrsys-Datron sensor to the car centre of gravity [m]	2.130	
No. of motors per axle (-)	2	
	Trailer A	Trailer B
Mass [kg]	1400	1000
Yaw mass moment of inertia [kgm^2]	778	646
Hitch joint to trailer centre of gravity distance [m]	2.666	1.961
Hitch joint to axle distance [m]	2.800	2.300

2.2. Vehicle model for control system design

A linearised single-track version of the model in (1) is used for control system design. The lateral axle forces are replaced by linear expressions, i.e., $F_{y,F} = C_F\alpha_F$, $F_{y,R} = C_R\alpha_R$, $F_{y,T} = C_T\alpha_T$, where C_i and α_i, with $i = F, R, T$, are the cornering stiffness and slip angle of the front axle of the towing car, the rear axle of the towing car and the trailer axle.

The cornering stiffness values were obtained from experimental skidpad tests carried out at the Lommel proving ground (Belgium), and were selected for a lateral acceleration of 5 m/s^2, following the approach in [47]. The test vehicle was the electric Range Rover Evoque prototype of the European FP7 project iCOMPOSE that towed a single-axle trailer, called trailer A in the remainder. During the model parameter identification tests, the TV controller was deactivated and the towing vehicle was operated with an equal torque distribution among the wheels, the so-called Passive vehicle configuration. Table 1 shows the main vehicle parameters together with two sets of trailer parameters. The control system design is based on the parameters of trailer A. As discussed in Section 6, the system performance was experimentally investigated with two trailers, trailer A and trailer B.

From (1) the system transfer functions, providing the states as functions of the inputs, are derived for the frequency domain analysis (see the appendix). In particular, the transfer functions $G_{M_{z,ref},r_C}(s) = \frac{r_C}{M_{z,ref}}(s)$ and $G_{M_{z,ref},\phi}(s) = \frac{\phi}{M_{z,ref}}(s)$ have the same fourth order denominator and different second order numerators.

2.3. Vehicle model for control system assessment

This study assesses the robustness and instability mitigation capability of the proposed TV controller with a high-fidelity articulated vehicle model implemented in IPG CarMaker. Previous studies [37] include the experimental validation of the towing vehicle model, i.e., the case study electric Range Rover Evoque; the trailer A model was developed from the data in Table 1. An experimental validation of the resulting articulated vehicle model was carried out for steady-state and transient conditions.

3. Hitch angle controllers

3.1. TV control structure with hitch angle feedback

Fig. 2 shows the feedback TV control structure with hitch angle control. The reference yaw moment is computed from a single control variable, Δr_ϕ, which is the weighted linear combination of the yaw rate error, Δr_C, and hitch angle error, $\Delta\phi$, where the latter has an influence only when it exceeds pre-determined thresholds:

$$\Delta r_\phi = K_\phi \Delta r_C - W_\phi\left(1 - K_\phi\right)\Delta\phi = K_\phi\left(r_{ref} - r_C\right) - W_\phi\left(1 - K_\phi\right)\Delta\phi \quad (12)$$

Saturations can be imposed on $\Delta\phi$ in (12), to limit the hitch angle contribution:

$$\Delta\phi = \begin{cases} \phi_{ref} - \phi, \ if\ \phi_{ref} - \phi \in \left[-\Delta\phi_{sat}; \Delta\phi_{sat}\right] \\ \Delta\phi_{sat} sign\left(\phi_{ref} - \phi\right), \ if\ \phi_{ref} - \phi \notin \left[-\Delta\phi_{sat}; \Delta\phi_{sat}\right] \end{cases} \quad (13)$$

The theoretical justification of this control structure is provided by [48], according to which the concurrent control of multiple variables, i.e., the yaw rate and hitch angle, with one input, i.e., the yaw moment applied to the towing vehicle, makes the system functionally uncontrollable. In other words, it is not possible to track both variables at the same time. Therefore, this study uses a novel single input single output (SISO) TV formulation, which is an extension of the one adopted in [41] for yaw rate and sideslip control in isolated vehicles.

To guard against driveability issues, the controller formulation includes threshold bands based on the hitch angle error $\phi_{ref} - \phi$, which allow gradually increasing the hitch angle correction. For small/negligible trailer oscillations, the weighting factor $1 - K_\phi$ is set to zero (i.e., $K_\phi = 1$) so that the controller only tracks the reference yaw rate of the car. If $|\phi_{ref} - \phi|$ is between predefined lower and upper thresholds, respectively $\Delta\phi_{th}$ and $\Delta\phi_{lim}$, the control action linearly blends the yaw rate and hitch angle errors. In formulas:

$$K_\phi = \begin{cases} 1, & if\ \phi_{ref} - \phi \in \left[-\Delta\phi_{th}; \Delta\phi_{th}\right] \\ 1 + \frac{K_{\phi,min} - 1}{\Delta\phi_{th} - \Delta\phi_{lim}}\left(\Delta\phi_{th} - \left|\phi_{ref} - \phi\right|\right), & if\ \phi_{ref} - \phi \in \left[-\Delta\phi_{lim}; -\Delta\phi_{th}\right] \cup \left[\Delta\phi_{th}; \Delta\phi_{lim}\right] \\ K_{\phi,min}, & if\ \phi_{ref} - \phi \notin \left[-\Delta\phi_{lim}; \Delta\phi_{lim}\right] \end{cases} \quad (14)$$

$K_{\phi,\,min}$ is usually set to a small positive value, thus allowing the driver or the automated driving controller to maintain an influence on the vehicle trajectory also during extreme oscillations of the trailer, which would not be the case for $K_{\phi,min} = 0$. The gain W_ϕ is included in (12) to provide an extra tuning parameter, which allows some degree of independent tuneability of the yaw rate and hitch angle loops.

The controller blends the yaw rate and hitch angle contributions only when the trailer dynamics are deemed critical. During normal driving, the controller tracks the reference yaw rate of the car. The parameters in (12)–(14) can be tuned directly on the vehicle demonstrator, or through optimisation routines accounting for model uncertainties, such as those associated with trailer mass and geometry, or the tyre-road friction coefficient. Owing to the availability of a vehicle demonstrator, the parameters used for the simulations and experimental tests of this preliminary study were determined directly on the proving ground.

According to the approach in [41], r_{ref}, i.e., the reference yaw rate of the towing vehicle, is the weighted average of the handling yaw rate,

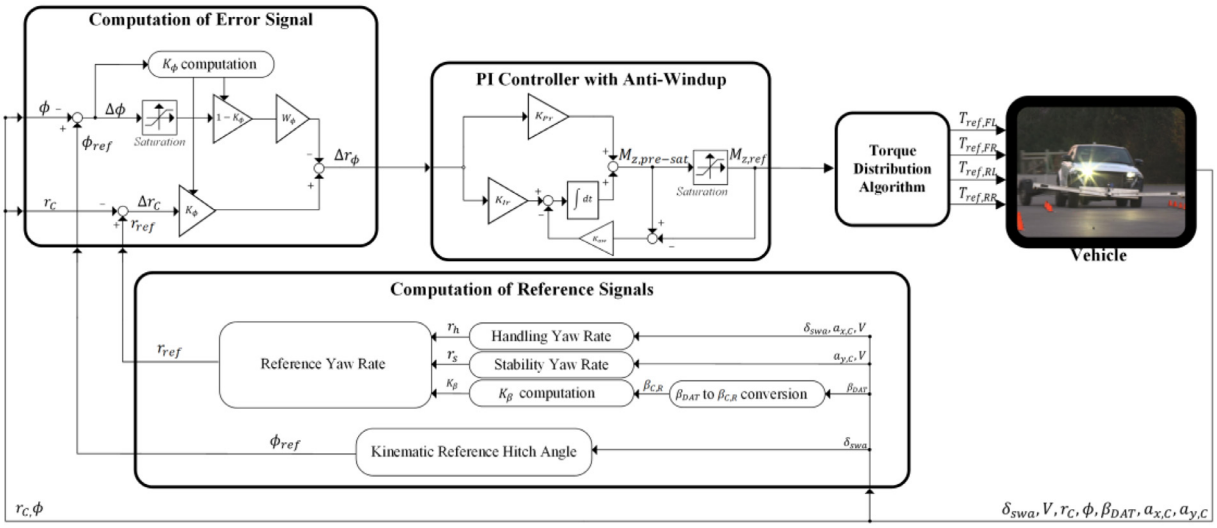

Fig. 2. Simplified block diagram of the proposed TV control structure.

r_h, and the stability yaw rate, r_s:

$$r_{ref} = (1 - K_\beta) r_h + K_\beta r_s \tag{15}$$

where r_h provides the reference behaviour in high tyre-road friction conditions, and depends on the driving mode selected by the driver, i.e., on the desired cornering response. This can be designed to obtain an understeer characteristic, i.e., the graph of steering wheel angle as a function of lateral acceleration, which is closer to the neutral steering behaviour and with higher maximum lateral acceleration or, vice versa, closer to the passive vehicle behaviour. The steady-state values of r_h are obtained from a look-up table for each driving mode, which is a function of steering angle and vehicle speed. The look-up tables are calculated offline with a quasi-static model and a set of reference understeer characteristics, as detailed in [36–38]. The look-up table output is low-pass filtered to provide the appropriate reference dynamics for r_h. r_s is computed from the measured lateral acceleration of the car, and represents a yaw rate value that is compatible with the available tyre-road friction conditions. The weighting factor, K_β, is a function of the rear axle sideslip angle, $\beta_{C,R}$, which can be either measured or estimated [38–39,49].

In this study the reference hitch angle, ϕ_{ref}, is the kinematic hitch angle, i.e., the hitch angle in absence of slip angles [50]. The differential equation describing the evolution of the kinematic hitch angle for a given vehicle speed, V, is:

$$\dot{\phi} = -\frac{V}{l_C}\left(\frac{l_C}{l_T}\sin(\phi) + \left(\frac{e_C}{l_T}\cos(\phi) + 1\right)\tan(\delta_w)\right) \tag{16}$$

By imposing $\dot{\phi} = 0$ in (16), it is:

$$\phi_{ref} = -\arctan\left(\frac{\tan(\delta_w)\left(l_c^2 l_T + e_C\sqrt{\tan^2(\delta_w) l_c^2 e_c^2 - \tan^2(\delta_w) l_c^2 l_T^2 + l_c^4}\right)}{l_C\left(-\tan^2(\delta_w) l_T e_C + \sqrt{\tan^2(\delta_w) l_c^2 e_c^2 - \tan^2(\delta_w) l_c^2 l_T^2 + l_c^4}\right)}\right) \tag{17}$$

In the controller ϕ_{ref} is used as an indicator of the expected steady-state hitch angle based on the driver input, for an average trailer geometry.

In accordance to the practice in stability control systems of production vehicles, this study adopts a Proportional Integral (PI) controller including an anti-windup scheme with gain K_{aw}:

$$M_{z,pre-sat} = K_{Pr}\Delta r_\phi + K_{Ir}\int \Delta r_\phi dt - K_{aw}\int \left(M_{z,pre-sat}(t^-) - M_{z,ref}(t^-)\right) dt \tag{18}$$

A specific algorithm is used for the online estimation of the maximum and minimum possible values of the direct yaw moment. The yaw moment limits are based on the wheel torque demand, the torque limits associated with the electric drivetrains, the estimated available tyre-road friction level at each corner, and (optionally) a fixed yaw moment level set up during the tuning phase of the controller. This allows the computation of the saturated yaw moment, $M_{z,ref}$, based on the most conservative condition, and provides an input to the torque distribution block. Given the significant change of the system dynamics with vehicle speed, the PI gains are scheduled with V. The torque distribution algorithm in Fig. 2 converts the vehicle torque demand from the drivability controller and the TV reference yaw moment into torque demands for the right and left sides of the vehicle, which are then evenly distributed between the front and rear drivetrains of each side.

3.2. Feedback controller design

The PI gains are selected for appropriate yaw rate control of the isolated car. A gain scheduling scheme is developed with the single-track model of the isolated car to keep constant stability margins of the yaw rate open-loop transfer function, $OLTF_{iso}(s) = G_{M_{z,ref},r_C,iso}(s) C_{PI}(s)$. For a selection of values of V, Table 2 reports: (i) the corresponding PI gains, K_{Pr} and K_{Ir}; (ii) the natural frequency and damping ratio of the rigid vehicle transfer function without TV control, i.e., $G_{M_{z,ref},r_C,iso}(s)$; and (iii) the gain and phase margins of $OLTF_{iso}(s)$.

The gains determined for the car are then used with the single-track model formulation of the articulated vehicle to verify that good stability margins are obtained for each control function: yaw rate control, i.e., $K_\phi = 1$, which implies $OLTF_{art,K_\phi=1}(s) = G_{M_{z,ref},r_C}(s) C_{PI}(s)$, and hitch angle control, i.e., $K_\phi = 0$, which implies $OLTF_{art,K_\phi=0}(s) = -W_\phi G_{M_{z,ref},\phi}(s) C_{PI}(s)$; note that the negative sign accounts for the adopted hitch angle convention.

Based on the experience of the authors, the selection of the TV system PI gains should be focused on the stability and disturbance rejection properties of the controller, rather than its tracking performance. In this way, the TV objectives can typically be achieved without compromising drivability, which is of the essence given the continuous operation of the TV controller. Nonetheless, in case a vehicle stability control functionality is pursued that only activates in emergency conditions, a tuning strategy focused on tracking performance could be adopted.

Table 2 shows the frequency response analysis data for different speeds, one set of PI gains and $W_\phi = 1$. f_n refers to the lowest value of natural frequency of the system, while ζ is the respective damping ratio. As indicated by the results, the set of gains determined for the rigid vehicle can be used for the TV controller of the articulated vehicles without compromising system stability. This observation allows

Table 2
Frequency response analysis for the articulated vehicle with TV controller, $i = r_C, \phi$.

V [km/h]	K_{Pr} [Nms/rad]	K_{Ir} [Nm/rad]	$G_{M_{z,ref},r_C,iso}(s)$		$OLTF_{iso}(s)$		$G_{M_{z,ref},\ i}\ (s)$		$OLTF_{art,K_\phi=1}$		$OLTF_{art,K_\phi=0}$	
			f_n [Hz]	ζ	Gain margin [dB]	Phase margin [deg]	f_n [Hz]	ζ	Gain margin [dB]	Phase margin [deg]	Gain margin [dB]	Phase margin [deg]
40	35,150	43,380	3.10	0.98	Inf	120	1.15	0.89	Inf	121	Inf	99
60	27,541	34,290	2.25	0.90	Inf	120	1.15	0.58	Inf	121	Inf	97
80	24,480	31,652	1.86	0.82	Inf	120	1.14	0.42	Inf	122	Inf	96
100	23,080	31,623	1.65	0.74	Inf	120	1.14	0.32	Inf	122	Inf	95

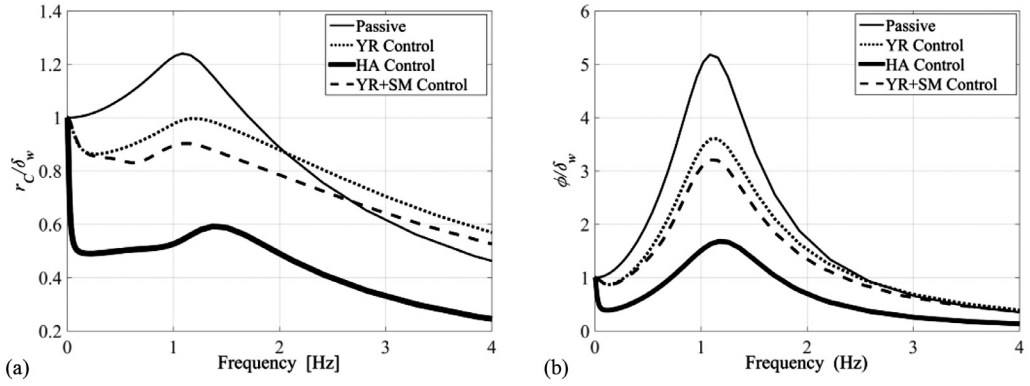

Fig. 3. Normalised frequency response of: (a) yaw rate; and (b) hitch angle to a steering input at $V = 100$ km/h.

a significant reduction of the control system tuning time. The stability of the gain scheduling scheme with respect to variations of V can be demonstrated with the method in [47].

3.3. Industrial controller

This section briefly presents the trailer sway mitigation algorithm patented by Bosch in [16], which was developed for cars with stability control systems based on the actuation of the friction brakes. A corrective yaw moment is applied when the estimated trailer oscillations exceed a certain level. Similarly to the TV controller (Section 3.1), the Bosch algorithm computes the reference yaw moment from a single control variable, which is the sum of the yaw rate error, Δr_C, and the filtered yaw rate error, $B(\Delta r_C)$, of the towing vehicle. The $B(\Delta r_C)$ contribution is considered only when the filter output exceeds a threshold value:

$$\Delta r_{C,filt,B} = \begin{cases} \Delta r_C + B(\Delta r_C), & if \left| B(\Delta r_C) \right| > threshold \\ \Delta r_C & otherwise \end{cases} \tag{19}$$

The filter is a second order Butterworth band-pass filter that is designed to isolate the oscillations in the yaw rate error signal caused by the trailer snaking:

$$B(z) = \frac{b_{B,0} + b_{B,1} z^{-1} + b_{B,2} z^{-2}}{a_{B,0} + a_{B,1} z^{-1} + a_{B,2} z^{-2}} \tag{20}$$

The coefficients of $B(z)$ are computed to provide cut-off frequencies of 0.375 Hz and 1.125 Hz. Then, the reference yaw moment can be generated with any feedback controller, by replacing Δr_C with $\Delta r_{C,\ filt,\ B}$ as control variable. In this study the PI formulation in (18) with the gains of Table 2 is used for the assessment of the trailer sway mitigation strategy.

4. Controller comparison

4.1. Frequency domain analysis

Fig. 3(a) and (b) compare the normalised frequency response of the yaw rate and hitch angle for a steering input at $V = 100$ km/h for:

- Passive – the passive articulated vehicle (without TV control and with even torque distribution) described by $G_{\delta_w,r_C}(s)$ and $G_{\delta_w,\phi}(s)$ (see appendix).
- YR Control – the articulated vehicle with TV control only on the yaw rate of the car ($K_\phi = 1$).
- HA Control – the vehicle with only the TV hitch angle control contribution active (i.e., $K_\phi = 0$).
  Note that in the following time domain analyses (see Sections 5 and 6), the TV controller with yaw rate and hitch angle control active is indicated as YR + HA Control. As described in Section 3, based on the variation of K_ϕ in the time domain, this configuration brings a closed-loop system behaviour that changes depending on the vehicle states.
- YR + SM Control – the industrial trailer sway mitigation (SM) controller with the Butterworth filter acting on the yaw rate error, which is added to the YR Control formulation, with B in (20) being converted into the Laplace domain.

The analysis assumes a linear relationship between the handling yaw rate and steering angle, where relevant. The normalisation of the Bode plots is carried out by dividing each transfer function by the respective steady-state gain. For a fair comparison, the PI gains of Table 2 were adopted for all active configurations. As shown by Fig. 3(b) all controllers can reduce the hitch angle resonance peak, with the HA Control being the most effective (reduction of 67.7% relative to Passive). The YR Control (reduction of 29.3%) and the YR + SM Control (reduction of 37.7%) provide similar benefits. Also, the results highlight the advantages of the flexibility of the YR + HA Control–the system response can be varied between that of the YR Control, focused on the enhancement

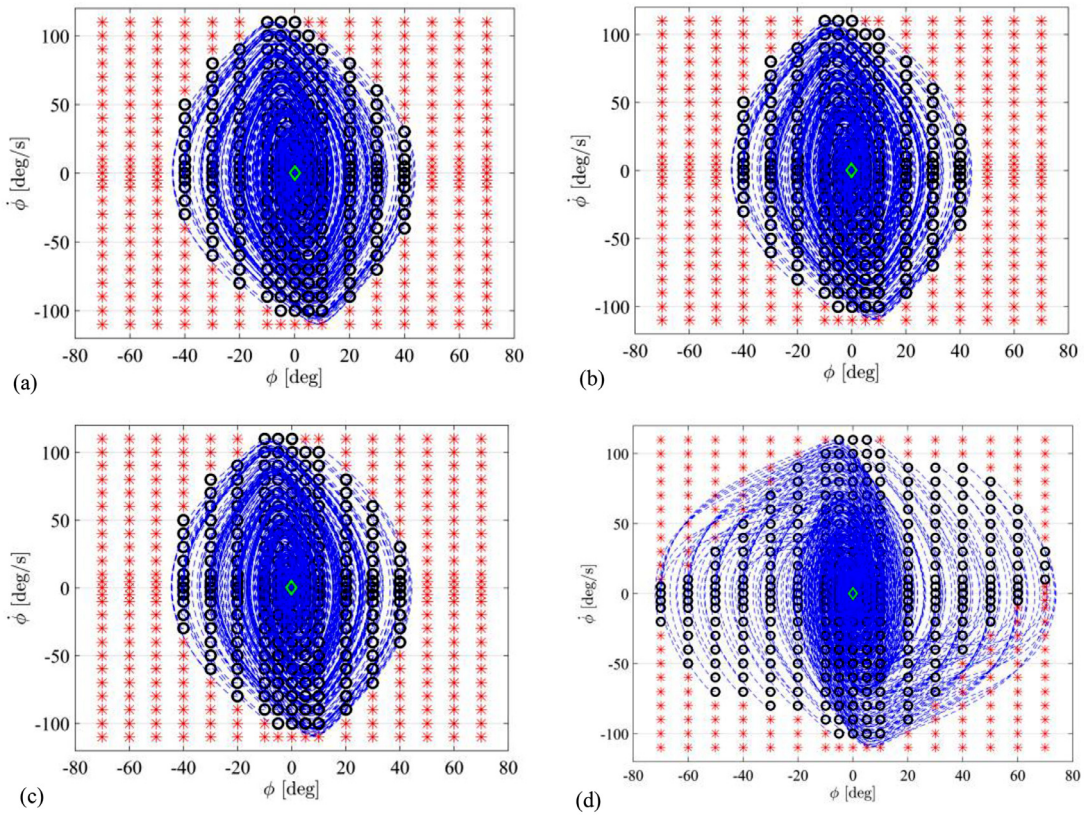

Fig. 4. Phase plane trajectories at $V = 100$ km/h and $\delta_w = 0$ deg for: (a) the passive vehicle; (b) the vehicle with the YR Control; (c) the vehicle with the YR + SM Control; and (d) the vehicle with the YR + HA Control.

of the towing vehicle response in steady-state and transient conditions for safety, performance and fun-to-drive, and that of the HA case, which provides a high damping of the hitch dynamics.

4.2. Phase plane analysis

The controllers of Section 3 are implemented into the nonlinear model of Section 2.1 to perform a phase plane analysis of the articulated vehicle response. The simulations are carried out at $V = 100$ km/h and $\delta_w = 0$ deg, and started with $r_C = \beta_C = 0$, while changing the initial conditions of ϕ and $\dot{\phi}$. For the analysis, the TV yaw moment is saturated at +/−5000 Nm. The parameters in (14) are $\Delta\phi_{th} = 4$ deg, $\Delta\phi_{lim} = 15$ deg and $K_{\phi,min} = 0$.

Fig. 4 reports the phase plane results. The star marker indicates a simulation run that exceeds the safety limits of the vehicle-trailer system, which are $|\dot{\phi}| \leq 110$ deg/s and $|\phi| \leq 75$ deg. These threshold values were selected by observing the behaviour of the passive vehicle during extreme manoeuvres in simulation. A successful run, i.e., when the $\dot{\phi}(\phi)$ trajectory remains within the assigned limits, is indicated with the open circle marker (at the initial condition coordinate) and the corresponding trajectory is shown in blue. Based on the limits, the passive vehicle can successfully complete 210 simulations, and the YR Control and the YR + SM Control vehicles finish 211 runs each. With 278 successful simulations, the vehicle with the YR + HA Control can complete ~32% more runs than the other vehicle cases.

Even in the cases exceeding the set limits, the proposed YR + HA Control stabilises the vehicle with reduced oscillations with respect to the other control configurations. The important and novel conclusion is that the direct adoption of the hitch angle information in the implementation of stability control systems would significantly enhance the active safety of car-trailer combinations.

Table 3
Tuning parameters of the hitch angle control function.

Parameter	Value
$\Delta\phi_{th}$	3 deg
$\Delta\phi_{lim}$	10 deg
W_{ϕ}	1 s^{-1}
$\Delta\phi_{sat}$	10 deg
$K_{\phi,\ min}$	0.1

5. Simulation results

The vehicle model of Section 2.3 is used to analyse the ability of the controller to cope with jackknifing and snaking. Furthermore, the analysis assesses the controller robustness with respect to large variations in model parameters, in particular: (i) trailer mass; (ii) longitudinal position of the trailer centre of gravity; and (iii) tyre-road friction coefficient. For conservativeness, in the next subsections the sideslip angle based correction of the reference yaw rate is deactivated. Therefore, the reference yaw rate only depends on the handling yaw rate, which is more aggressive than the response of the passive vehicle. In addition, the tuning parameters of the hitch angle control function, reported in Table 3, are kept constant in all simulations.

5.1. Jackknifing scenario

Jackknifing is a very common instability mode of articulated vehicles, in which the towing vehicle reaches the friction limit and the trailer does not. The momentum of the latter pushes the towing vehicle, which

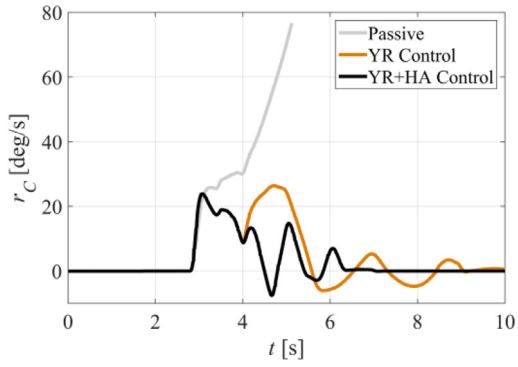

Fig. 5. Towing vehicle yaw rate during a jackknifing scenario simulation.

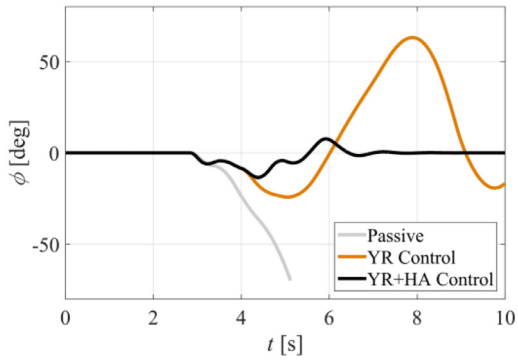

Fig. 6. Hitch angle during a jackknifing scenario simulation.

ultimately spins. The articulated vehicle finally ends up in a "folded" position [8].

To simulate this scenario, the tyre-road friction coefficient μ is set to 0.6. The vehicle is accelerated to a speed of 100 km/h. Then the accelerator pedal is released and a swift steering wheel input with a 100 deg magnitude is imposed at a rate of 400 deg/s. At the same time, a strong force impulse is applied to the brake pedal. This only affects the braking system of the towing vehicle, which consequently tends to spin. After 2 s, the steering wheel angle is brought back to zero with a gradient of −400 deg/s.

Figs. 5 and 6 show the time histories of the yaw rate of the towing vehicle and hitch angle for: (i) the passive case; (ii) the vehicle with only the YR Control; and (iii) the vehicle with the proposed YR + HA Control. The simulation is purposely designed to induce jackknifing in the passive vehicle (grey lines in the plots) and understand the TV controller reaction. Interestingly, in order to follow the reference yaw rate, the YR Control applies a large positive yaw moment at ∼4 s, which increases the yaw rate of the car but also has a negative effect on the trailer, as indicated by the large increase in hitch angle. By this point the vehicle has been subjected to a significant speed reduction, which increases damping and helps stabilisation. In the simulation with the YR + HA Control, as the trailer motion increases beyond the activation thresholds of the hitch angle safety function, a negative yaw moment is generated between 4 s and 5 s, which decreases the towing vehicle yaw rate and helps maintaining trailer stability. All subsequent trailer oscillations are easily dealt with by the controlled vehicle, which ultimately recovers the straight-line motion at ∼7 s in Fig. 5, significantly earlier and at higher final speed than with the YR Control.

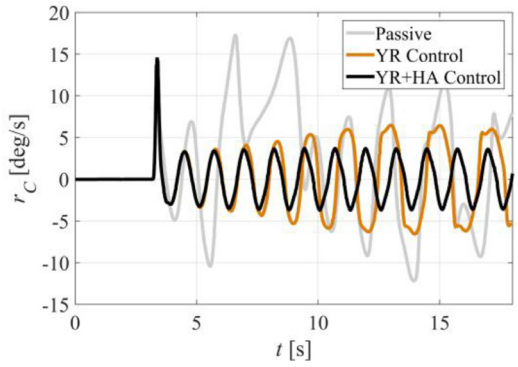

Fig. 7. Towing vehicle yaw rate during a snaking scenario simulation.

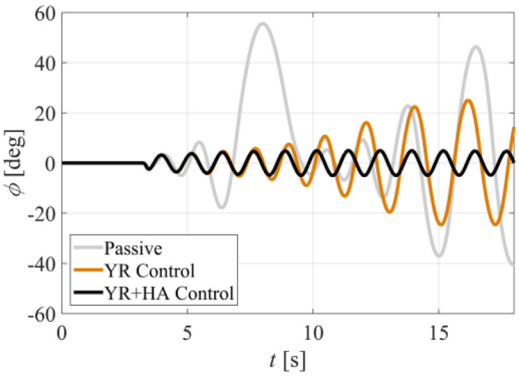

Fig. 8. Hitch angle during a snaking scenario simulation.

5.2. Snaking scenario

Snaking occurs when the trailer begins oscillating in a self-amplifying fashion [9]. This can happen when the trailer parameters cause system instability from a control viewpoint, i.e., at least one of the eigenvalues of the system has positive real part. As soon as the system is subjected to a small input or an external disturbance, the instability causes the oscillation of the hitch angle to progressively increase until, ultimately, the vehicle cannot be recovered.

In the snaking simulation, μ is set to 1 and the trailer axle is moved forward, to be closer to the hitch joint than the trailer centre of gravity. The vehicle is accelerated up to a speed of 100 km/h. Then a constant wheel torque demand is set and a steering wheel impulse of ∼40 deg magnitude is applied, which induces the trailer oscillations.

Figs. 7 and 8 show the snaking scenario results. After a few seconds, in the passive case the trailer exhibits large amplitude oscillations, which also correspond to towing vehicle oscillations, as indicated by the yaw rate profile. As a consequence, the vehicle loses speed, which increases system damping and reduces the hitch angle oscillations. The situation improves with the YR Control. As the steering angle is zero after the steering impulse, the reference yaw rate is zero, which implies that the TV controller tries to keep the car in a straight line. Despite this, the oscillations quickly build up as shown by the yaw rate and hitch angle time histories. After a significant drop in vehicle speed, the situation stabilises at ∼15 s. In the YR + HA simulation, the amplitude of the hitch angle oscillations initially increases similarly to the YR case. As soon as the hitch angle error threshold is exceeded, the controller starts correcting the trailer motion. Because of the unstable nature of the specific trailer configuration, and the fact that the controller is designed to only correct the hitch angle if the threshold is exceeded, the hitch angle does not asymptotically tend to 0 deg, but is kept within reasonable values. By setting the activation threshold to 0 deg, it would be possible

Table 4
Sensitivity analyses during sinusoidal steer test at $V = 70$ km/h.

Sensitivity on m_T			Sensitivity on a_T			Sensitivity on μ		
m_T [kg]	Passive $RMSE_{\Delta\phi}$ [deg]	YR + HA $RMSE_{\Delta\phi}$ [deg]	a_T [m]	Passive $RMSE_{\Delta\phi}$ [deg]	YR + HA $RMSE_{\Delta\phi}$ [deg]	μ [-]	Passive $RMSE_{\Delta\phi}$ [deg]	YR + HA $RMSE_{\Delta\phi}$ [deg]
400	1.58	1.48	2.5	6.13	2.52	1	8.94	3.01
1400	10.20	3.01	2.7	8.94	3.01	0.8	16.88	4.45
2400	x	6.70	3.1	x	6.20	0.6	x	6.29
3400	x	12.50	3.3	x	11.54	0.4	x	5.08
4400	x	x	3.5	x	x	0.2	x	x

x: loss of vehicle stability.

to have hitch angle convergence; however, this is not the purpose of the controller, specifically designed to intervene in critical conditions.

5.3. Sensitivity analyses

The sensitivity analyses compare the response of the passive vehicle and the vehicle with the YR + HA Control function during a sinusoidal steering test. The vehicle is accelerated up to a speed of 70 km/h; then a constant wheel torque demand of 500 Nm is set and a single sinusoidal steering wheel input of 50 deg magnitude is applied, which provokes a swinging motion of the trailer. This is also one of the manoeuvres adopted in the experimental assessment of the controller. The sensitivity analysis is conducted by changing each parameter individually. The simulation results are in Table 4, which includes the values of $RMSE_{\Delta\phi}$, i.e., the root mean square value of the hitch angle error:

$$RMSE_{\Delta\phi} = \sqrt{\frac{1}{t_f - t_i}\int_{t_i}^{t_f} \Delta\phi^2 dt} \tag{21}$$

$RMSE_{\Delta\phi}$ is an indicator of the hitch angle deviation from its reference behaviour.

The results of the sensitivity analysis on trailer mass show that not only the YR + HA Control improves vehicle behaviour with respect to the passive configuration, but also that the trailer mass can be increased by 2000 kg in the active vehicle (from 1400 kg to 3400 kg) before stability issues occur because of actuator saturation. In the analysis on the trailer COG position, as expected, for both the passive and active vehicles the $RMSE_{\Delta\phi}$ worsens when the trailer centre of gravity is moved rearward. The YR + HA Control can keep stability when the COG is by 0.5 m more rearward than in the passive case. The last scenario assesses the effect of the tyre-road friction coefficient. The YR + HA Control can maintain vehicle stability in a wider range of road conditions, and at the same time always generates better response than for the passive case.

These results could be further improved by: (i) the activation of the sideslip angle stability function; and (ii) the adaptive variation of the TV controller parameters, which were purposely kept constant in this preliminary analysis.

6. Experimental results

6.1. Experimental set-up

To experimentally assess the performance of the TV systems with YR Control and YR + HA Control, the algorithms (Section 3) were implemented on the dSpace AutoBox rapid control prototyping unit of the battery electric Range Rover Evoque vehicle demonstrator (Fig. 9) mentioned in Section 2. The vehicle is equipped with four identical on-board electric drivetrains and an electro-hydraulic braking system to allow precise individual wheel control in traction and braking. The controllers were tested with two different single axle trailers, trailer A and trailer B, that differ in length and mass; trailer A is heavier and has a greater hitch-to-axle distance (Table 1). Both trailers have conventional overrun braking systems, actuated by a mechanism located on the drawbar.

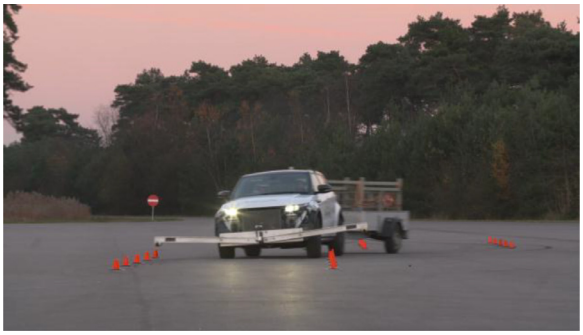

Fig. 9. The vehicle demonstrator with trailer A during an obstacle avoidance test at the Lommel proving ground.

The sensor setup included: (i) two inertial measurement units (IMUs), installed in the car and on the trailer to measure their respective yaw rate and lateral acceleration; (ii) a Corrsys-Datron S-350 sensor attached to the front bumper of the car to measure the body sideslip angle. The sideslip angle values at the centre of gravity and at the rear axle of the car were computed by considering the measured yaw rate; and (iii) a potentiometer connecting the car and the trailer to determine the hitch angle.

The vehicle tests were performed at the Lommel proving ground (Belgium) with the three system configurations (see Sections 4 and 5)– Passive, YR Control, and YR + HA Control. For each test the vehicle was accelerated up to the target speed and, then, a constant torque demand was set and maintained throughout the rest of the manoeuvre. The torque demand was approximately equal to the resistance torque for straight line driving at the reference speed. Four manoeuvres were performed:

i) Single sinusoidal steering test with a steering wheel angle input of 50 deg amplitude and 3 s duration, starting at $V_{in} = 70$ km/h.
ii) Sweep steering test with a sinusoidal steering wheel input at a progressively increasing frequency and 20 deg amplitude, starting at $V_{in} = 90$ km/h.
iii) Prolonged sinusoidal steering test at constant frequency and 20 deg amplitude, starting at $V_{in} = 90$ km/h.
iv) Obstacle avoidance test, in which the vehicle has to complete the manoeuvre without hitting cones positioned according to the ISO standard 3888–2 [51].

In the following subsections, unless otherwise specified, the parameters of the hitch angle stability function used in the controller are those reported in Table 3.

6.2. Single sinusoidal steering test

Figs. 10–12 show the time histories of steering wheel angle, hitch angle and yaw rate measured during the single sinusoidal steering test. As indicated by Fig. 11, this manoeuvre significantly excites the trailer

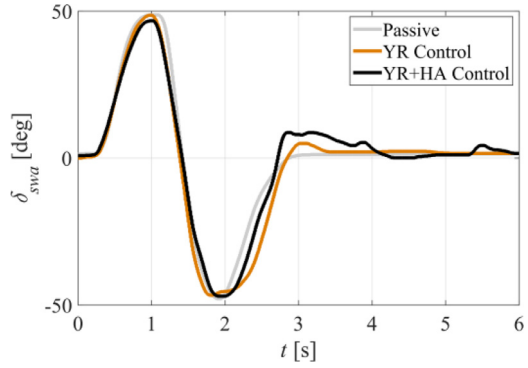

Fig. 10. Steering wheel angle during sinusoidal steering test with trailer A and $V_{in} = 70$ km/h, for three different vehicle configurations.

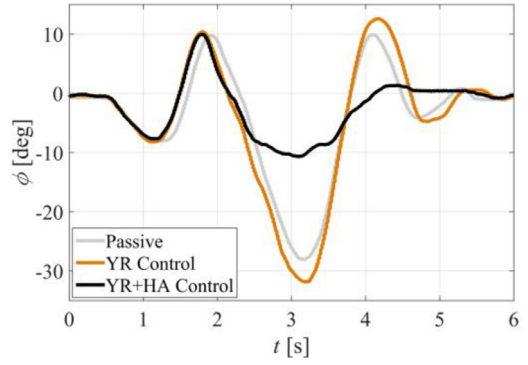

Fig. 11. Hitch angle during sinusoidal steering test with trailer A and $V_{in} = 70$ km/h, for three different vehicle configurations.

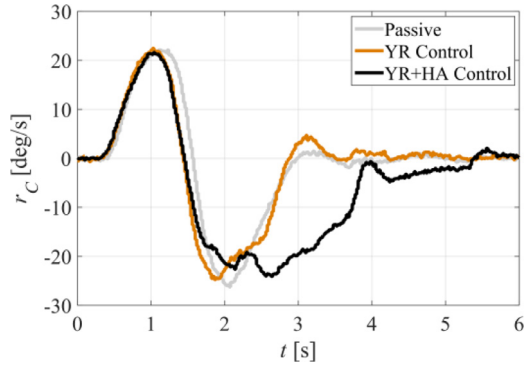

Fig. 12. Yaw rate of the car during sinusoidal steering test with trailer A, $V_{in} = 70$ km/h, and three different vehicle configurations.

dynamics. The Passive and YR Control configurations experience maximum hitch angles of ~30 deg at $t \approx$ 3.2 s. The similar behaviour of the two vehicle configurations is due to the fact that the towing car remains within its cornering limits, i.e., with a maximum lateral acceleration of 8 m/s^2. Hence, $r_{ref}(t)$ is close to $r_C(t)$, so that the magnitude of $M_{z,\,ref}$ computed by the YR Control is rather low and hardly influences the vehicle behaviour. This observation also confirms the simulation results of Section 4 and 5 that showed the marginal benefit of the YR Control compared to the passive vehicle. In contrast, with the YR + HA Control configuration the hitch angle correction is activated at $t \approx$ 2.4 s, i.e., when $|\Delta\phi| > \Delta\phi_{th} = 3$ deg. As a result, the TV system dampens the trailer yaw dynamics and $\phi(t)$ is kept bounded to a low amplitude of ~10 deg. However, the yaw moment associated with the hitch angle contribution

Table 5
Performance indicators for the sinusoidal tests with trailer A.

	Passive	YR control	YR + HA control
$RMSE_{\Delta\phi}$ [deg]	10.05	11.95	4.67
$RMSE_{\Delta r_C}$ [deg/s]	4.82	2.36	9.74
$RMSE_{\Delta r_\phi}$ [deg/s]	10.31	11.43	8.49
$\lvert\phi_{max}\rvert$ [deg]	28.02	31.82	10.65
$IACA$ [Nm]	–	820	2051

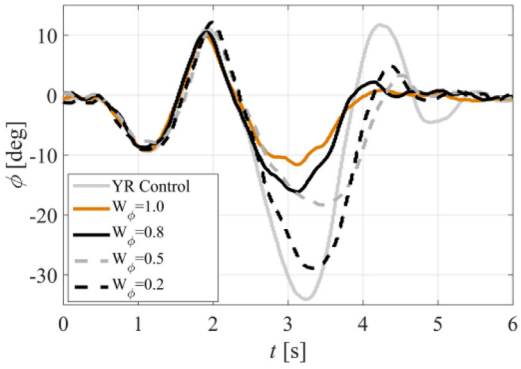

Fig. 13. Hitch angle during sinusoidal steering test with trailer A and $V_{in} = 70$ km/h, for YR Control and for YR + HA Control with different values of W_ϕ [1/s].

makes the car maintain a negative yaw rate even when the steering input is returning to zero. Although this effect is an intrusion into the driver control action on vehicle trajectory, the feedback from the professional test drivers on the vehicle behaviour was positive, as the trailer oscillations experienced with the Passive and YR Control configurations were perceived as rather critical.

To quantitatively assess the system behaviour, the following performance indicators were computed and are reported in Table 5:

- The root mean square error values, *RMSE*, of $\Delta\phi$, Δr_C and Δr_ϕ, based on the definition in (21).
- The maximum absolute value of the hitch angle during the test, $|\phi_{max}|$.
- The integral of the absolute value of the control action, *IACA*:

$$IACA = \frac{1}{t_f - t_i} \int_{t_i}^{t_f} \left| M_{z,ref} \right| dt \tag{22}$$

The highest $RMSE_{\Delta r_C}$ value (Table 5) indicates that the YR + HA Control vehicle has the lowest yaw rate tracking performance. However, the hitch angle tracking performance significantly improves (see the $RMSE_{\Delta\phi}$ value) and $|\phi_{max}|$ is more than halved, compared to the other two configurations. Also, as the overall articulated vehicle is operating in less critical conditions, the $RMSE_{\Delta r_\phi}$ value reduced, which implies an overall better performance of the feedback controller. As expected, the damping of the trailer oscillations by the YR + HA Control was achieved through a considerably higher control effort; in fact, the *IACA* value of the YR + HA Control is nearly 2.5 times greater than with the YR Control setup.

To assess the tuneability of the YR + HA Control, two experimental sensitivity analyses based on the sinusoidal steering test were conducted – one on W_ϕ, and one on $\Delta\phi_{th}$ and $\Delta\phi_{lim}$. Fig. 13 shows the hitch angle time histories obtained with the different W_ϕ settings, including the YR Control configuration ($W_\phi = 0$). As indicated by the results, the hitch angle peak can be reduced by increasing W_ϕ. Fig. 14 shows the hitch angle error time histories, $\Delta\phi(t)$, for different $\Delta\phi_{th}$ and $\Delta\phi_{lim}$ values and the YR Control case. As expected, the experiments show that lower threshold values anticipate the controller activation and lead to a considerable

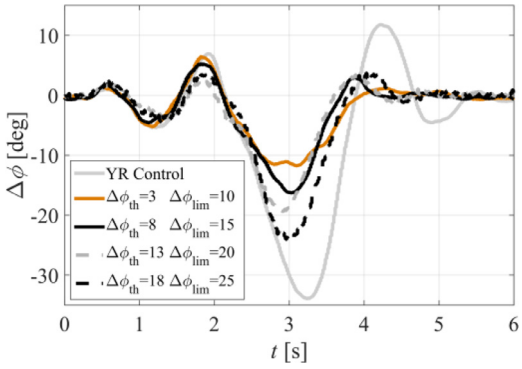

Fig. 14. Hitch angle error during sinusoidal steering test with trailer A and V_{in} = 70 km/h, for YR Control and for YR + HA Control with different values of $\Delta\phi_{th}$ and $\Delta\phi_{lim}$ [deg].

Table 6
Maximum frequency, f_{max}, of the steering wheel input during the sweep steering tests with trailer A.

	Passive	YR Control	YR + HA Control
f_{max} [Hz]	0.5	0.6	1.1

reduction in trailer sway, as opposed to a more oscillating behaviour when the thresholds are more relaxed.

6.3. Frequency sweep steering test

The frequency sweep steering test was carried out to investigate the lateral stability of the vehicle-trailer system with the developed controllers. As indicated by the test results, the Passive vehicle (Fig. 15(a) & (d)) and the YR Control vehicle (Fig. 15(b) & (e)) exhibit resonance behaviour at similar steering frequencies, approx. 0.5 Hz and 0.6 Hz, see Table 6. Therefore, it was not possible to safely achieve a higher frequency and the driver had to stop the manoeuvre. With the YR + HA Control (Fig. 15(c) & (f)), the driver was able to increase the input frequency well beyond the level of the other two configurations, as the trailer resonance condition was damped by the yaw moment correction performed by the hitch angle contribution. The maximum steering frequency achieved in this test was 1.1 Hz. Higher frequencies would have been possible with a consistently good safety margin, but the test road was not sufficiently long to safely continue the manoeuvre.

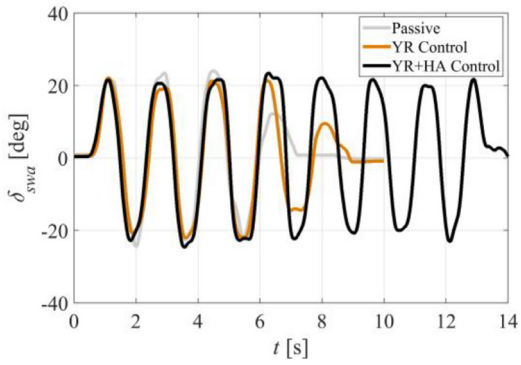

Fig. 16. Steering wheel angle during sinusoidal steering test with trailer A, steering frequency of 0.67 Hz and V_{in} = 90 km/h for three different vehicle configurations.

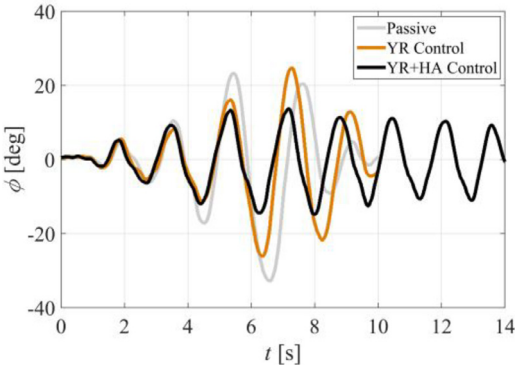

Fig. 17. Hitch angle during sinusoidal steering test with trailer A, steering frequency of 0.67 Hz and V_{in} = 90 km/h for three different vehicle configurations.

6.4. Prolonged sinusoidal steering test at constant frequency

The prolonged sinusoidal steering test was carried out at a steering frequency of 0.67 Hz in order to excite the trailer dynamics (see Section 6.3). As indicated by Figs. 17 and 18, this test provoked critical driving conditions with the Passive and YR Control vehicle configurations. In particular, the oscillations of the trailer increased beyond a safe

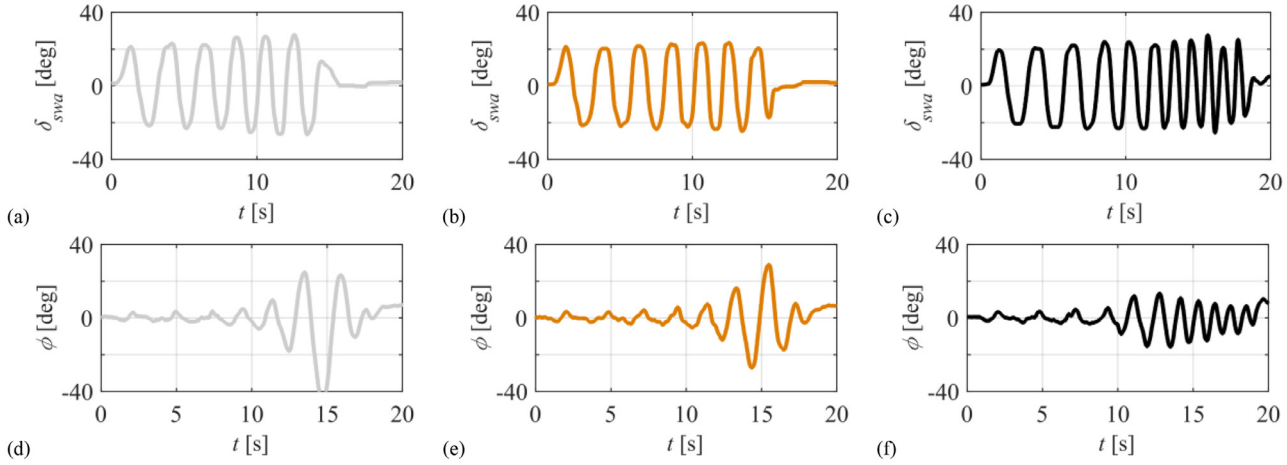

Fig. 15. Steering wheel angle (a, b, c) and hitch angle (d, e, f) profiles for: the Passive vehicle (a, d); the vehicle with the YR Control (b, e); and the vehicle with the YR + HA Control (c, f) during sweep steering test with trailer A and V_{in} = 90 km/h.

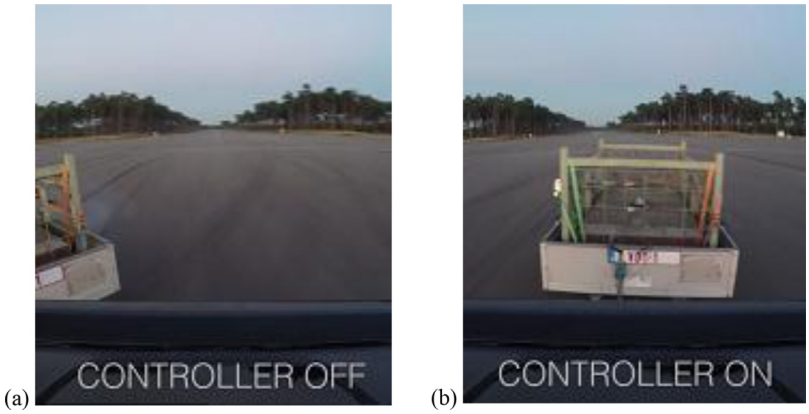

Fig. 18. Rear-view camera shot of trailer A during the sinusoidal steering test at a steering frequency of 0.67 Hz and V_{in} = 90 km/h for: (a) the Passive vehicle; and (b) the vehicle with the YR + HA Control.

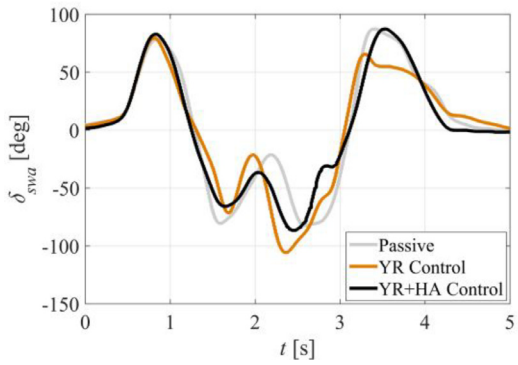

Fig. 19. Steering wheel angle during obstacle avoidance test with trailer B and V_{in} = 50 km/h.

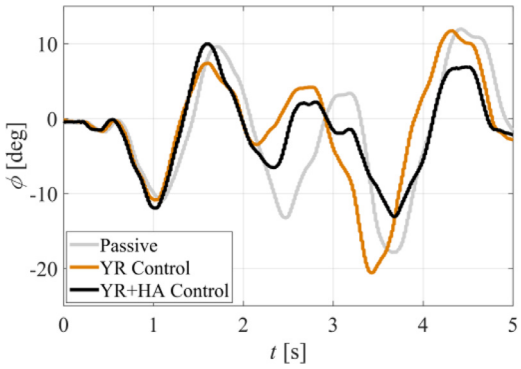

Fig. 20. Hitch angle during obstacle avoidance test with trailer B and V_{in} = 50 km/h.

level (Fig. 17) and the driver had to abort the manoeuvre early ($\delta_{swa}(t)$ reduced to zero at approx. 7 s and 9 s, see Fig. 16) and slow down the car. In contrast, with the YR + HA Control the trailer oscillations had a small amplitude and were bounded (Fig. 17), so that the test could safely continue and be completed. This result indicates the significant safety enhancement that can be achieved with the YR + HA Control. Also, the on-board shots taken at the maximum amplitude of trailer oscillations with the Passive and YR + HA Control cases visually demonstrate the potential safety benefit of the controlled vehicle (Fig. 18).

6.5. Obstacle avoidance test

The obstacle avoidance test was carried out with trailer B, which is lighter and shorter than trailer A. To allow a preliminary assessment of the controller robustness, the experiments were carried out with the tuning parameter set established with trailer A.

During the first part of the manoeuvre (see Figs. 19 and 20), the quick transition from the first to the second lane brings a progressive increase in trailer sway. When the vehicle returns to the first lane at $t \approx$ 3 s, the trailer is still oscillating and the rapid change of direction provokes further oscillations, leading to the hitch angle peaks at $t \approx$ 3.5 s and $t \approx$ 4.5 s. In the second half of the manoeuvre, which is the critical part of the test, the YR + HA Control significantly reduces the oscillation amplitude with respect to the other two configurations. Moreover, it allows successful completion of the manoeuvre, i.e., no cone is hit, which was not the case for the Passive and the YR Control vehicles.

Fig. 21 compares the maximum initial speeds that still allow successful completion of the test. In each assessed configuration, the vehicle had 5 attempts to complete the course without hitting cones. If the attempt

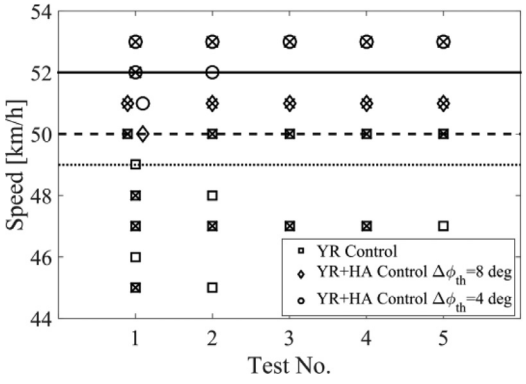

Fig. 21. Map of the obstacle avoidance test results with trailer B for different control configurations and initial speeds.

was successful, the speed was increased by 1 km/h and the manoeuvre was repeated until 5 consecutive failures occurred from the same initial speed. In Fig. 21, the open maker indicates a successful attempt and the "x" indicates an unsuccessful attempt. The horizontal lines highlight the maximum initial speeds achieved by the vehicle with: (i) the YR Control (dotted line); (ii) the YR + HA Control with $\Delta\phi_{th}$ = 8 deg and $\Delta\phi_{lim}$ = 15 deg; (iii) the same controller as in (ii) but with $\Delta\phi_{th}$ = 4 deg (solid line). Configuration (i) achieved a maximum speed of 49 km/h, while the YR + HA Control allowed to increase the maximum speed up to 50 km/h in configuration (ii), and to 52 km/h in configuration (iii).

Fig. 22 shows aerial views of the vehicle during tests from 49 km/h. With the Passive configuration (Fig. 22(a)), the trailer swings to the left-hand side of the car (negative hitch angle peak) and, in doing so, hits

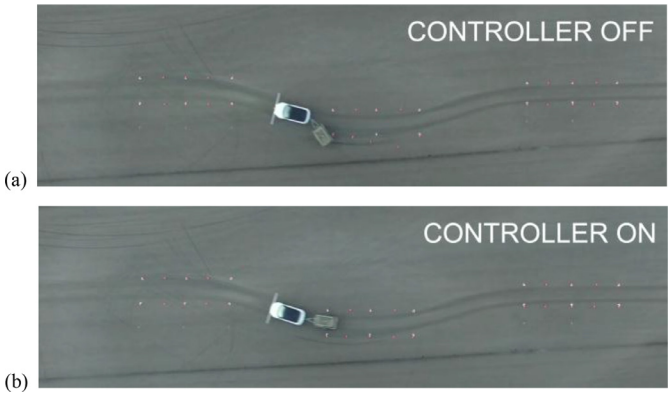

Fig. 22. Aerial view of obstacle avoidance tests with trailer B for (a) the passive vehicle; and (b) the vehicle with the YR + HA Control.

several cones. With the YR + HA Control (case (ii)) the trailer oscillates to the left (see Fig. 22(b)) and the hitch angle error is negative. Based on the controller formulation in Section 3, this condition reduces the yaw moment, which, then, leads to a decrease in the yaw rate of the car. As a result, the car is heading more to the right in reaction to the sway of the trailer to the left, the oscillations are reduced and no cone is hit.

7. Conclusions

The novel TV control setup of this study – the YR + HA Control – combines the simplicity of a SISO structure (which facilitates industrial implementation) with the capability of: (i) shaping the understeer characteristic of the car through continuous yaw rate tracking; (ii) indirectly constraining the sideslip angle of the car by modifying its reference yaw rate; and (iii) indirectly limiting the hitch angle oscillations through a control variable that considers yaw rate and hitch angle errors.

The main conclusions are:

- A TV system based only on the yaw rate and sideslip angle of the car (i.e., without special consideration of the trailer dynamics) cannot provide significant active safety benefits when a trailer is towed.
- The phase plane analysis with the nonlinear vehicle model demonstrated the significant extension of the safe vehicle operating conditions allowed by the YR + HA Control (up to 32%), compared to: (i) an industrial trailer sway mitigation function with a band-pass filter on the car yaw rate error; and (ii) the TV system based only on the yaw rate and sideslip angle of the car.
- The good performance of the YR + HA Control was confirmed by the frequency domain analysis. With respect to the benchmark industrial controller, the YR + HA Control reduced the hitch angle resonance amplitude by up to 48%.
- The simulation results with the high-fidelity vehicle model showed the YR + HA Control robustness with respect to: (i) jackknifing and snaking; and (ii) large variations in model parameters, i.e., location of the trailer centre of gravity, trailer mass and tyre-road friction coefficient.
- The YR + HA Control allowed bounding of the system response of the case study vehicle-trailer combinations to safe levels throughout the sinusoidal steering and obstacle avoidance tests of this study.
- The experimental sensitivity analyses highlighted the predictable tuneability of the YR + HA Control algorithm, which facilitates quick set up of the controller.

The very promising experimental results encourage further research on the definition of industrially implementable methods for the direct measurement or state estimation of the hitch angle in car-trailer combinations.

Declaration of Competing Interest

The authors declare that they have no known competing financial interests or personal relationships that could have appeared to influence the work reported in this paper.

Acknowledgement

The research leading to these results has received funding from the European Union Seventh Framework Programme FP7/2007-2013 under Grant Agreement no. 608897 (iCOMPOSE project).

Appendix

The transfer functions of the single-track model of the articulated vehicle are:

$$G_{\delta_w,r_C}(s) = \frac{r_C}{\delta_w}(s) = \frac{N_{3\delta_w,r_C}s^3 + N_{2\delta_w,r_C}s^2 + N_{1\delta_w,r_C}s^1 + N_{0\delta_w,r_C}}{D(s)} \tag{A1}$$

$$G_{\delta_w,\beta_C}(s) = \frac{\beta_C}{\delta_w}(s) = \frac{N_{3\delta_w,\beta_C}s^3 + N_{2\delta_w,\beta_C}s^2 + N_{1\delta_w,\beta_C}s^1 + N_{0\delta_w,\beta_C}}{D(s)} \tag{A2}$$

$$G_{\delta_w,\phi}(s) = \frac{\phi}{\delta_w}(s) = \frac{N_{2\delta_w,\phi}s^2 + N_{1\delta_w,\phi}s^1 + N_{0\delta_w,\phi}}{D(s)} \tag{A3}$$

$$G_{M_{z,ref},r_C}(s) = \frac{r_C}{M_{z,ref}}(s) = \frac{N_{3M_{z,ref},r_C}s^3 + N_{2M_{z,ref},r_C}s^2 + N_{1M_{z,ref},r_C}s^1 + N_{0M_{z,ref},r_C}}{D(s)} \tag{A4}$$

$$G_{M_{z,ref},\beta_C}(s) = \frac{\beta_C}{M_{z,ref}}(s) = \frac{N_{3M_{z,ref},\beta_C}s^3 + N_{2M_{z,ref},\beta_C}s^2 + N_{1M_{z,ref},\beta_C}s^1 + N_{0M_{z,ref},\beta_C}}{D(s)} \tag{A5}$$

$$G_{M_{z,ref},\phi}(s) = \frac{\phi}{M_{z,ref}}(s) = \frac{N_{2M_{z,ref},\phi}s^2 + N_{1M_{z,ref},\phi}s^1 + N_{0M_{z,ref},\phi}}{D(s)} \tag{A6}$$

$$D(s) = D_4s^4 + D_3s^3 + D_2s^2 + D_1s^1 + D_0 \tag{A7}$$

where the coefficients are:

$$D_0 = -\Big(\big(\big(\big(\big(a_C + h_C\big)m_T + m_C a_C\big)C_F - \big(\big(b_C - h_C\big)m_T + m_C b_C\big)C_R\big)l_T - a_T\big(C_F\big(a_C + h_C\big) - C_R\big(b_C - h_C\big)\big)m_T\big)V^2 - C_F C_R l_T\big(a_C + b_C\big)^2\Big)C_T V \tag{A8}$$

$$\begin{aligned} D_1 = {} & \big(\big(-\big(\big(\big(-a_c - h_c\big)C_F + C_R\big(b_c - h_c\big)\big)l_T + C_F\big(a_c + hc\big)\big(a_c + a_T + h_c\big) - \big(b_c - h_c\big)\big(-b_c + a_T + h_c\big)C_R\big)\big(a_T - l_T\big)m_T \\ & -m_c\big(C_F a_c - C_R b_c\big)l_T^2 + \big(\big(b_c^2 m_c + J_{z,c}\big)C_R + C_F\big(a_c^2 m_c + J_{z,c}\big)\big)l_T - \Big(C_F\big(a_c + h_c\big) - C_R\big(b_c - h_c\big)\Big)J_{z,T}\Big)V^2 + C_F C_R l_T^2\big(a_c + b_c\big)^2\Big)C_T \end{aligned} \tag{A9}$$

$$\begin{aligned} D_2 = {} & -\Big(\Big(\Big(-\big(a_c + h_c\big)^2\big(a_T + l_T\big)C_F - \big(b_c - h_c\big)^2\big(a_T - l_T\big)C_R + V^2\big(h_c^2 m_c + J_{z,c}\big)\Big)\big(a_T + l_T\big)m_T \\ & +\big(-J_{z,c}h_c^2 - 2J_{z,T}a_c h_c + \big(-a_c^2 m_c - J_{z,c}\big)l_T^2 - J_{z,T}a_c^2\big)C_F \\ & +\big(-J_{z,c}h_c^2 + 2J_{z,T}b_c h_c + \big(-b_c^2 m_c - J_{z,c}\big)l_T^2 - J_{z,T}b_c^2\big)C_R - V^2 m_c J_{z,c}l_T\big)C_T \\ & +\Big(\Big(-a_T^2\big(a_c + b_c\big)^2 C_R + \big(J_{z,T}h_c + a_c\big(a_T^2 m_c + J_{z,T}\big)\big)V^2\Big)C_F - \big(-J_{z,T}h_c + b_c\big(a_T^2 m_c + J_{z,T}\big)\big)C_R V^2\Big)m_T \\ & +J_{z,T}\Big(\Big(-\big(a_c + b_c\big)^2 C_R + V^2 m_c a_c\Big)C_F - V^2 m_c C_R b_c\Big)\Big)V \end{aligned} \tag{A10}$$

$$\begin{aligned} D_3 = {} & \Big(\Big(J_{z,T}\big(\big(C_F + C_R\big)h_c^2 + \big(2C_F a_c - 2C_R b_c\big)h_c + a_c^2 C_F + b_c^2 C_R\big) + \Big(\big(a_T - l_T\big)^2 C_T + a_T^2\big(C_F + C_R\big)\Big)J_{z,c} \\ & +\Big(h_c^2\big(a_T - l_T\big)^2 C_T + a_T^2\big(C_F a_c^2 + C_R b_c^3\big)m_c\Big)m_T + \big(\big(C_F + C_R + C_T\big)J_{z,c} + m_c\big(C_F a_c^2 + C_R b_c^2 + C_T h_c^2\big)\big)J_{z,T} + m_c J_{z,c}C_T l_T^2\big)V^2 \end{aligned} \tag{A11}$$

$$D_4 = V^3\big(\big(\big(m_C + m_T\big)J_{z,T} + {a_T}^2 m_C m_T\big)J_{z,C} + {h_C}^2 m_C m_T J_{z,T}\big) \tag{A12}$$

$$N_{0\delta_w,r_C} = C_F V^2 C_R C_T l_T\big(a_C + b_C\big) \tag{A13}$$

$$N_{1\delta_w,r_C} = C_F C_T\big(\big(\big(\big(m_C + m_T\big)a_C + m_T h_C\big)l_T - m_T a_T\big(a_C + h_C\big)\big)V^2 + C_R {l_T}^2\big(a_C + b_C\big)\big)V \tag{A14}$$

$$N_{2\delta_w,r_C} = \Big(\Big(\big(a_T - l_T\big)^2\big(a_C + h_C\big)m_T + \big({l_T}^2 m_C + J_{z,T}\big)a_C + J_{z,T}h_C\Big)C_T + C_R\big(a_C + b_C\big)\big({a_T}^2 m_T + J_{z,T}\big)\Big)C_F V^2 \tag{A15}$$

$$N_{3\delta_w,r_C} = C_F\big(\big(\big(m_C + m_T\big)a_C + m_T h_C\big)J_{z,T} + a_C {a_T}^2 m_C m_T\big)V^3 \tag{A16}$$

$$N_{0\delta_w,\beta_C} = -C_F C_T\big(\big(\big(\big(m_C + m_T\big)a_C + m_T h_C\big)l_T - m_T a_T\big(a_C + h_C\big)\big)V^2 - C_R b_C l_T\big(a_C + b_C\big)\big)V \tag{A17}$$

$$N_{1\delta_w,\beta_C} = -\Big(\Big(\big(\big(a_C + h_C\big)m_T + m_C a_C\big){l_T}^2 + \Big(-2\big(a_C + h_C\big)\Big(a_T + \frac{1}{2}h_C\Big)m_T - J_{z,C}\Big)l_T + \big(J_{z,T} + m_T a_T\big(a_T + h_C\big)\big)\big(a_C + h_C\big)\Big)V^2 - C_R b_C {l_T}^2\big(a_C + b_C\big)\Big)C_F C_T \tag{A18}$$

$$N_{2\delta_w,\beta c} = -\Big(\Big(-h_c\big(a_T - l_T\big)^2\big(a_c + h_c\big)C_T + \big(V^2 J_{z,T} + a_T^2\big(V^2 m_c - C_R b_c\big)\big)a_c - C_R a_T^2 b_c^2 + V^2 J_{z,T} h_c\Big)m_T + \big(-J_{z,c} l_T^2 - J_{z,T} a_c h_c - J_{z,T} h_c^2\big)C_T + J_{z,T}\big(\big(V^2 m_c - C_R b_c\big)a_c - b_c^2 C_R\big)\big)C_F V \tag{A19}$$

$$N_{3\delta_w,\beta} = C_F\big(\big(h_C\big(a_C + h_C\big)m_T + J_{z,C}\big)J_{z,T} + {a_T}^2 m_T J_{z,C}\big)V^2 \tag{A20}$$

$$N_{0\delta_w,\phi} = -\big(\big(C_R {l_T}^2\big(a_C + b_C\big) + \big(-\big(b_C - h_C\big)\big(a_C + b_C\big)C_R + \big(\big(m_C + m_T\big)a_C + m_T h_C\big)V^2\big)l_T - V^2 m_T a_T\big(a_C + h_C\big)\big)C_T - V^2 m_T C_R a_T\big(a_C + b_C\big)\big)C_F V \tag{A21}$$

$$N_{1\delta_w,\phi} = -\Big(\Big(\big(a_T - l_T\big)^2\big(a_C + h_C\big)C_T + C_R a_T\big(-b_C + a_T + h_C\big)\big(a_C + b_C\big)\Big)m_T + \big(\big(h_C l_T m_C + {l_T}^2 m_C + J_{z,T}\big)a_C - J_{z,C} l_T + J_{z,T} h_C\big)C_T + J_{z,T} C_R\big(a_C + b_C\big)\Big)C_F V^2 \tag{A22}$$

$$N_{2\delta_w,\phi} = -\big(\big(\big({a_T}^2 m_C + a_T m_C h_C + J_{z,T}\big)a_C - a_T J_{z,C} + h_C J_{z,T}\big)m_T + m_C J_{z,T} a_C\big)C_F V^3 \tag{A23}$$

$$N_{0M_{z,ref},r_C} = \big(C_F + C_R\big)C_T l_T V^2 \tag{A24}$$

$$N_{1M_{z,ref},r_C} = -V\big(\big(-C_F - C_R\big){l_T}^2 - V^2\big(m_C + m_T\big)l_T + m_T a_T V^2\big)C_T \tag{A25}$$

$$N_{2M_{z,ref},r_C} = \Big(\Big(\big(a_T - l_T\big)^2 m_T + {l_T}^2 m_C + J_{z,T}\Big)C_T + \big(C_F + C_R\big)\big({a_T}^2 m_T + J_{z,T}\big)\Big)V^2 \tag{A26}$$

$$N_{3M_{z,ref},r_C} = V^3\big(\big(m_C + m_T\big)J_{z,T} + {a_T}^2 m_C m_T\big) \tag{A27}$$

$$N_{0M_{z,ref},\beta_C} = V\big(\big(-\big(m_C + m_T\big)V^2 - a_C C_F + b_C C_R\big)l_T + m_T a_T V^2\big)C_T \tag{A28}$$

$$N_{1M_{z,ref},\beta_C} = -\Big(\Big(\big(m_C + m_T\big){l_T}^2 - 2\Big(a_T + \frac{1}{2}h_C\Big)m_T l_T + m_T a_T\big(h_C + a_T\big) + J_{z,T}\Big)V^2 + {l_T}^2\big(a_C C_F - b_C C_R\big)\Big)C_T \tag{A29}$$

$$N_{2M_{z,ref},\beta_C} = -V\big(\big(V^2 J_{z,T} + \big(V^2 m_C + a_C C_F - b_C C_R - C_T h_C\big){a_T}^2 + 2C_T h_C l_T a_T - C_T h_C {l_T}^2\big)m_T + J_{z,T}\big(V^2 m_C + a_C C_F - b_C C_R - C_T h_C\big)\big) \tag{A30}$$

$$N_{3M_{z,ref},\beta_C} = J_{z,T} V^2 h_C m_T \tag{A31}$$

$$N_{0M_{z,ref},\phi} = -V\big(\big(\big(C_F + C_R\big){l_T}^2 + \big(\big(m_C + m_T\big)V^2 + \big(h_C + a_C\big)C_F - \big(b_C - h_C\big)C_R\big)l_T - m_T a_T V^2\big)C_T - V^2 m_T a_T\big(C_F + C_R\big)\big) \tag{A32}$$

$$N_{1M_{z,ref},\phi} = -V^2\big(\big(\big(C_F + C_R + C_T\big){a_T}^2 + \big(-2l_T C_T + \big(h_C + a_C\big)C_F - \big(b_C - h_C\big)C_R\big)a_T + C_T {l_T}^2\big)m_T + \big(h_C l_T m_C + {l_T}^2 m_C + J_{z,T}\big)C_T + J_{z,T}\big(C_F + C_R\big)\big) \tag{A33}$$

$$N_{2M_{z,ref},\phi} = -\big(\big(J_{z,T} + m_T a_T\big(h_C + a_T\big)\big)m_C + J_{z,T} m_T\big)V^3 \tag{A34}$$

References

[1] Kang X, Deng W. Vehicle-trailer handling dynamics and stability control–an engineering review; 2007. SAE Technical Paper No. 2007-01-0822.
[2] van de Molengraft-Luijten MFJ, Besselink IJM, Verschuren RMAF, Nijmeijer H. Analysis of the lateral dynamic behaviour of articulated commercial vehicles. Veh Syst Dyn 2012;50(sup1):169–89.
[3] Ding N, Shi X, Zhang Y, Chen W, Shi X, Zhang Y, Chen W. Analysis of bifurcation and stability for a tractor semi-trailer in planar motion. Veh Syst Dyn 2014;52(12):1729–51.
[4] Crolla DA, Hales FD. The lateral stability of tractor and trailer combinations. J Terramech 1979;16(1):1–22.
[5] Bao J, Jin-liang L, Yan Y. Lateral stability analysis of the tractor/full trailer combination vehicle. IEEE International Conference on Electric Information and Control Engineering (ICEICE); 2011.
[6] Sharp RS, Fernández MA. Car-caravan snaking: part 1 - The influence of pintle-pin friction. Proc Inst Mech Eng, Part C 2002;216(7):707–22.
[7] Bouteldja M, Cerezo V. Jackknifing warning for articulated vehicles based on a detection and prediction system. 3rd International Conference on Road Safety and Simulation; 2011.
[8] Bouteldja M, Koita A, Dolcemascolo V, Cadiou JC. Prediction and detection of jackknifing problems for tractor semi-trailer. IEEE Vehicle Power and Propulsion Conference; 2006.
[9] Azad NL, Khajepour A, McPhee J. Stability control of articulated steer vehicles by passive and active steering systems; 2005. SAE Technical Paper No. 2005-01-3573.
[10] Darling J, Tilley D, Gao B. An experimental investigation of car-trailer high-speed stability. Proc Inst Mech Eng, Part D 2009;223(4):471–84.
[11] Šušteršič G, Prebil I, Ambrož M. The snaking stability of passenger cars with light cargo trailers. Strojniški vestnik 2014;60(9):539–48.
[12] Daimler A.G., How Trailer Stability Assist works, daimler.com, 2018. [Online]. Available: http://media.daimler.com/marsMediaSite/en/instance/ko/The-technology-How-Trailer-Stability-Assist-works.xhtml?oid=9904516. [Accessed: 23 April 2018].
[13] Honda New Zealand, New technology page. [Online]. Available: https://www.honda.co.nz/technology/safety/tsa/. [Accessed: 21 23 April 2018].
[14] Skoda, Trailer stability assist. 2017. [Online]. Available: http://www.skoda.am/models/hotspotdetail?HotspotName=S05%20-%20TSA%20%5BOctavia%2C%20Yeti%2C%20Superb%5D&WebID=d7bed316-b6e4-470d-b39f-c90dfacc400b&Page=technology&view=TechnologySafety&WebPartID=&PageUrl=/sites/en-am/models/superb/pages/technology.aspx. [Accessed: 21 November 2017].
[15] E. Gerum, P. Laszlo, A. Semsey, G. Barta, Method for drive stability enhancement of multi-unit vehicles. U.S. Patent No. 5,747,683 (1998).
[16] H. Wu, F. Nardi, J. Chen, E. Hartman, Closed-loop control for trailer sway mitigation, U.S. Patent No. 8,740,317 (2014).
[17] Williams JM, Mohn FW. Trailer stabilization through active braking of the towing vehicle; 2004. SAE Technical Paper No. 2004-01-1069.
[18] Hac A, Fulk D, Chen H. Stability and control considerations of a vehicle-trailer combination. SAE Int J Passeng Cars-Mech Syst 2008;1:925–37 2008-01-1228.
[19] Mokhiamar O, Abe M. Examination of different models following types of yaw moment control strategy for improving handling safety of a car–caravan combination. Proc Inst Mech Eng, Part D 2003;217(7):561–71.
[20] Mokhiamar O. Stabilization of car-caravan combination using independent steer and drive/or brake forces distribution. Alex Eng J 2015;54(3):315–24.
[21] Deng W, Kang X. Parametric study on vehicle-trailer dynamics for stability control; 2003. SAE Technical Paper No. 2003-01-1321.
[22] Fernández MA, Sharp RS. Caravan active braking system - Effective stabilisation of snaking of combination vehicles; 2001. SAE Technical Paper No. 2001-01-3188 p. 1–12.
[23] Sharp RS, Fernández MA. Car-caravan snaking: part 2 - Active caravan braking. Proc Inst Mech Eng, Part C 2002;216(7):723–36.
[24] Plöchl M, Lugner P, Riepl A. Improvements of passenger car-trailer behaviour by a trailer based control system. Veh Syst Dyn 1998;29(S1):438–50.
[25] Tabatabaei Oreh SH, Kazemi R, Azadi S. A new desired articulation angle for directional control of articulated vehicles. Proc Inst Mech Eng, Part K 2012;226(4):298–314.
[26] Lee E, Kapoor S, Sikder T, He Y. An optimal robust controller for active trailer differential braking systems of car-trailer combinations. Int J Veh Syst Model Test 2017;12(1–2):72–93.
[27] Shamim R, Islam MM, He Y. A comparative study of active control strategies for improving lateral stability of car-trailer systems; 2011. SAE Technical Paper No. 2011-01-0959 p. 1–13.
[28] Oh P, Zhou H, Pavlov K. Stability control of combination vehicle; 2001. SAE Technical Paper No. 2001-01-0138.
[29] Tamaddoni SH, Taheri S. Yaw stability control of tractor semi-trailers; 2008. SAE Technical Paper No. 2008-01-2595.
[30] Ei-Gindy M, Mrad N, Tong X. Sensitivity of rearward amplification control of a truck/full trailer to tyre cornering stiffness variations. Proc Inst Mech Eng, Part D 2001;215(5):579–88.
[31] Kim K, Guan H, Guan B, Guo R, Liang F. Active steering control strategy for articulated vehicles. Front Inf Technol Electron Eng 2016;17:576–86.
[32] K. Englert, D. Mersden, E. Chubb, D. Messih, P. Schmitt, Trailer sway control with trailer brake intervention, U.S. Patent No. 9,834,187 (2017).
[33] Wang W, Fan J, Xiong R, Sung F. Lateral stability control of four wheels independently drive articulated electric vehicle. IEEE Transportation Electrification Conference and Expo; 2016.
[34] Chen LK, Shieh YA. Jack-knife prevention for articulated vehicles using model reference adaptive control. Proc Inst Mech Eng, Part D 2011;225(1):28–42.
[35] Wang Y, Nguyen BM, Fujimoto H, Hori Y. Multirate estimation and control of body sideslip angle for electric vehicles based on onboard vision system. IEEE Trans Ind Electron 2014;61(2):1133–43.
[36] De Novellis L, Sorniotti A, Gruber P. Driving modes for designing the cornering response of fully electric vehicles with multiple motors. Mech Syst Signal Process 2015;64-65:1–15.
[37] De Novellis L, Sorniotti A, Gruber P. Wheel torque distribution criteria for electric vehicles with torque-vectoring differentials. IEEE Trans Veh Technol 2014;63(4):1593–602.
[38] De Novellis L, Sorniotti A, Gruber P, Orus J, Fortun JMR, Theunissen J, De Smet J. Direct yaw moment control actuated through electric drivetrains and friction brakes: theoretical design and experimental assessment. Mechatronics 2015;26:1–15.
[39] Lu Q, Gentile P, Tota A, Sorniotti A, Gruber P, Costamagna F, De Smet J. Enhancing vehicle cornering limit through sideslip and yaw rate control. Mech Syst Signal Process 2016;75:455–72.
[40] Dizqah AM, Lenzo B, Sorniotti A, Gruber P, Fallah S, De Smet J. A fast and parametric torque distribution strategy for four-wheel drive energy efficient electric vehicles. IEEE Trans Ind Electron 2016;63(7):4367–76.
[41] Lenzo B, Sorniotti A, Gruber P, Sannen K. On the experimental analysis of single input single output feedback control of yaw rate and sideslip angle. Int J Automot Technol 2017;18(5):799–811.
[42] H. Wu, Trailer sway mitigation using torque vectoring, U.S. Patent No. 9,061,663 (2015).
[43] Vempaty S, He Y. A review of car-trailer lateral stability control approaches; 2017. SAE Technical Paper No. 2017-01-1580.
[44] Genta G. Motor vehicle dynamics: modeling and simulation, 43. 1st ed. World Scientific; 1997.
[45] Pacejka H. Tyre and vehicle dynamics. 3rd ed. Elsevier; 2012.
[46] Milliken WF, Milliken DL. Race car vehicle dynamics. 1st ed. SAE International; 1995.
[47] Lu Q, Sorniotti A, Gruber P, Theunissen J, De Smet J. H∞ loop shaping for the torque-vectoring control of electric vehicles: theoretical design and experimental assessment. Mechatronics 2016;35:32–43.
[48] Skogestad S, Postlethwaite I. Multivariable feedback control. 2nd ed. Wiley; 2005.
[49] Doumiati M, Victorino AC, Charara A, Lechner D. Onboard real-time estimation of vehicle lateral tire–road forces and sideslip angle. IEEE/ASME Trans Mechatron 2011;16(4):601–14.
[50] Rill G. Road vehicle dynamics: fundamentals and modelling. 1st ed. CRC Press; 2011.
[51] ISO 3888-2:2011. Passenger cars-Test track for a severe lane-change manoeuvre. Part 2: Obstacle avoidance. BSI Standard; 2011.

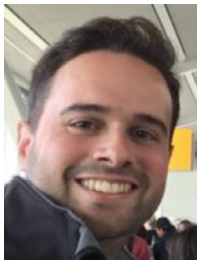

Mattia Zanchetta received the B.Sc. degree in electronic engineering and telecommunications and the M.Sc. degree in control engineering from the University of Pavia, Pavia, Italy, in 2013 and 2016, respectively. He is now a PhD researcher at the University of Surrey, Guildford, U.K. His research interests include vehicle dynamics and control, and autonomous driving.

Davide Tavernini received the M.Sc. degree in mechanical engineering and Ph.D. degree in dynamics and design of mechanical systems from the University of Padova, Padua, Italy, in 2010 and 2014. During his Ph.D. he was part of the motorcycle dynamics research group. He is a Lecturer in advanced vehicle engineering with the University of Surrey, Guildford, U.K. His research interests include vehicle dynamics modelling and control, mostly applied to electric and hybrid electric vehicles.

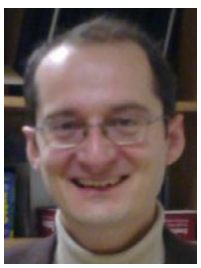

Aldo Sorniotti received the M.Sc. degree in mechanical engineering and Ph.D. degree in applied mechanics from the Politecnico di Torino, Turin, Italy, in 2001 and 2005, respectively. He is a Professor in advanced vehicle engineering with the University of Surrey, Guildford, U.K., where he coordinates the Centre for Automotive Engineering. His research interests include vehicle dynamics control and transmission systems for electric and hybrid vehicles.

Patrick Gruber received the M.Sc. degree in motorsport engineering and management from Cranfield University, Cranfield, U.K., in 2005, and the Ph.D. degree in mechanical engineering from the University of Surrey, Guildford, U.K., in 2009. He is a Reader in advanced vehicle systems engineering with the University of Surrey. His current research interests include vehicle and tyre dynamics, and the development of novel tyre and rubber friction models.

Basilio Lenzo received the M.Sc. degree in mechanical engineering from the University of Pisa and the Scuola Superiore Sant'Anna, Pisa, Italy, in 2010, and the Ph.D. degree in robotics from the Scuola Superiore Sant'Anna in 2013. In 2015 and 2016 he was a Research Fellow with the University of Surrey, Guildford, U.K. He is a Senior Lecturer in automotive engineering with Sheffield Hallam University, Sheffield, U.K. His research interests include vehicle dynamics, simulation, control, and robotics.

Antonella Ferrara received the M.Sc. degree in electronic engineering and the Ph.D. degree in computer science and electronics from the University of Genoa, Genoa, Italy, in 1987 and 1992, respectively. Since 2005, she has been a Full Professor of automatic control with the University of Pavia, Pavia, Italy. Her main research interests include sliding mode control applied to automotive systems, process control, and robotics.

Koen Sannen received the B.Eng. degree in automotive engineering from HAN University of Applied Sciences, the Netherlands, and the M.Sc. degree in automotive engineering from Oxford Brookes University, U.K., in 2008 and 2009, respectively. He is currently a Research and Test Engineer with Flanders Make, Lommel, Belgium.

Jasper De Smet received the M.Sc. degree in electrical engineering from the Katholieke Universiteit (KU) Leuven (Campus De Nayer), Sint-Katelijne-Waver, Belgium, in 2008. After graduation, he had a one-year internship with Eurocopter, Marignane, France. Since 2009, he has been a Researcher with Flanders MAKE, Lommel, Belgium. His research interests include integration and control of electromechanical systems in vehicles and machines.

Wouter De Nijs received the M.Sc. degree in mechanical engineering in the field of mechatronics from the KU Leuven, Leuven, Belgium, in 2006. He is a Core Lab Manager with Flanders Make, the Flemish Strategic Research Centre for the Manufacturing Industry, Leuven, Belgium, where his lab performs pre-competitive industry driven research on novel sensing, monitoring, control and decision making solutions in the application fields of vehicles-, machines- and factories-of-the-future.